Preprint typeset in JHEP style - HYPER VERSION INT-PUB-11-012; January 18, 2013

Universality of Phases in QCD and QCD-like Theories

Masanori Hanada[a] **and Naoki Yamamoto**[b]

[a] *Department of Physics, University of Washington, Seattle, WA 98195-1560, USA*
[b] *Institute for Nuclear Theory, University of Washington, Seattle, Washington 98195-1550, USA*
Email: mhanada@u.washington.edu, nyama@u.washington.edu

Abstract: We argue that the whole or the part of the phase diagrams of QCD and QCD-like theories should be universal in the large-N_c limit through the orbifold equivalence. The whole phase diagrams, including the chiral phase transitions and the BEC-BCS crossover regions, are identical between SU(N_c) QCD at finite isospin chemical potential and SO($2N_c$) and Sp($2N_c$) gauge theories at finite baryon chemical potential. Outside the BEC-BCS crossover regions in these theories, the phase diagrams are also identical to that of SU(N_c) QCD at finite baryon chemical potential. We give examples of the universality in some solvable cases: (i) QCD and QCD-like theories at asymptotically high density where the controlled weak-coupling calculations are possible, (ii) chiral random matrix theories of different universality classes, which are solvable large-N (large volume) matrix models of QCD. Our results strongly suggest that the chiral phase transition and the QCD critical point at finite baryon chemical potential can be studied using sign-free theories, such as QCD at finite isospin chemical potential, in lattice simulations.

Keywords: QCD phase diagram, Large-N_c QCD, Orbifold equivalence, BEC-BCS crossover, Chiral random matrix theory.

Contents

1. Introduction

Unraveling the properties of quantum chromodynamics (QCD) at finite temperature T and finite baryon chemical potential μ_B is essential to understand various phenomena from ultrarelativistic heavy-ion collisions, the early Universe, supernova explosion, and neutron stars, to possible quark stars (for a recent review, see, e.g., [1]). A lot of progress have been made theoretically by the first-principles lattice simulations in QCD at high T and sufficiently small μ_B in connection with the experimental investigation of the quark-gluon plasma in the ultrarelativistic heavy-ion collisions at RHIC and LHC. On the other hand, the lattice technique is not available at finite μ_B because of the *sign problem*: the fermion determinant is no longer real at finite μ_B, and the Monte Carlo approach based on the importance sampling does not work. This is why QCD at finite μ_B has not been fully understood, such as the precise location of the QCD critical point(s) (for a review, see [2]) and the realization of the color superconductivity at intermediate μ_B (for a review, see [3]) relevant to the physics of neutron stars, etc.

Still there are a class of QCD-like theories which are free from the sign problem. These theories intensively studied so far include two-color QCD with even numbers of fundamental flavors [4, 5], any-color SU(N_c) QCD with adjoint fermions [5], and SU(N_c) QCD at finite isospin chemical potential μ_I [6, 7]. In addition to the chiral phase transition, these theories exhibit the Bardeen-Cooper-Schrieffer (BCS) pairing of quarks at large chemical potential due to the same mechanism as the color superconductivity in real QCD [3]. However, it is not clear, at the quantitative level, or even at the qualitative level, how the phase diagrams of these theories are related to each other, and more importantly, to that of real QCD at finite μ_B. There are also other theories which are free from sign problem at finite μ_B but have not been well studied: SO($2N_c$) and Sp($2N_c$) gauge theories with N_f fundamental Dirac fermions.[1] Apparently, there is no a priori reason why these theories capture the physics of SU(N_c) QCD at finite chemical potential either, since the structures of gauge groups are different.

In this paper, we argue that the whole or the part of the phase diagrams of QCD and QCD-like theories should be *universal* in the large-N_c limit via the orbifold equivalence.[2] The relations between QCD and QCD-like theories are summarized in Fig. 1. The whole phase diagrams described by the chiral condensate and the superfluid gap should be quantitatively identical between SU(N_c) QCD at finite μ_I and SO($2N_c$) and Sp($2N_c$) gauge theories at finite μ_B.[3] As common properties of these theories, the Bose-Einstein conden-

[1] The symplectic group is defined as $\mathrm{Sp}(2N_c) = \{g \in \mathrm{U}(2N_c) | g^T J_c g = J_c\}$, where J_c is the antisymmetric matrix defined in (2.10). The dimension of Sp($2N_c$) is $N_c(2N_c+1)$.

[2] The universality of the Wilson loops between SU(N_c), SO($2N_c$), and Sp($2N_c$) in pure gauge theories in the large-N_c limit was pointed out long time ago in [8], even before the notion of the orbifold equivalence was found. Probably the first paper which considered an equivalence of the phase diagrams of QCD-like theories is [9], in which SU(N_c) gauge theory with two index fermion representations [adjoint, (anti)symmetric, and bifundamental] on the compact space $S^1 \times S^3$ as a function of volume was studied. Our paper is the first, to our knowledge, to argue the large-N_c universality of the phase diagrams of QCD and sign-free SO($2N_c$) and Sp($2N_c$) gauge theories with fundamental fermions at finite chemical potential on physically relevant space $\mathbb{R}^4$.

[3] We note that the deconfinement phase transition characterized by the Polyakov loop should also be

sate (BEC) of the Nambu-Goldstone (NG) modes at small chemical potential, as well as the BCS-type pairing at large chemical potential, appear in the phase diagrams. Since the BEC and BCS pairings carry the same quantum numbers and break the same symmetry, the BEC and BCS regions should be continuously connected without any phase transition. This is the BEC-BCS crossover similar to that in nonrelativistic condensed-matter systems [10, 11, 12] and the continuity between the hadron phase and the color superconducting phase (hadron-quark continuity) in three-flavor QCD at finite μ_B [13, 14, 15].[4] The universality of the phase diagrams means that both the chiral phase transitions and the BEC-BCS crossover regions should appear at the same coordinates in the T-μ plane independently of the theories in spite of the different symmetry breaking patterns.

We also argue that the phase diagrams of these theories outside the BEC-BCS crossover regions should be identical to that of SU(N_c) QCD at finite μ_B, which is most relevant in reality. In particular, the magnitude and temperature dependence of the chiral condensate in QCD at finite μ_B should be exactly the same as those in QCD at finite μ_I. Since the latter can be obtained by dropping the complex phase of the fermion determinant in the former for even number of flavors, this suggests that the phase-quenched approximation for the chiral condensate is exact in this region. Actually, this phenomenon has already been observed in the lattice QCD simulations [19] and the model calculations, such as the chiral random matrix model [20], the Nambu–Jona-Lasinio model [21, 22], and the hadron resonance gas model [23], though the reason has been unclear so far. We note that our arguments based on the orbifold equivalence are model-independent (though it is exact in the large-N_c limit), and thus, would provide a solid theoretical basis of the phase-quenched approximation.

The idea of the orbifold equivalence first originates from the string theory [24, 25, 26], and then has been generalized to the quantum field theory without reference to the string theory [27, 28, 29, 30, 31, 32, 33, 34]. The procedure of orbifolding (or orbifold projection) is as follows. Identify a discrete global symmetry of the original theory (the "parent" theory). Eliminate all the degrees of freedom in the parent theory which are not invariant under the discrete symmetry. This gives a new theory (the "daughter" theory). Then a class of correlation functions and observables are shown to be identical between the parent and daughter theories in the large-N_c limit, as long as the symmetry used to make the projection is not broken [32]. For example, as recently proposed [35, 36], SU(N_c) QCD with N_f quarks at finite μ_B can be obtained from the SO($2N_c$) gauge theory with N_f

identical between these theories. Because the quark chemical potential μ does not affect the gauge dynamics as long as $\mu = \mathcal{O}(N_c^0)$ in the large-N_c counting, the deconfinement temperature is independent of μ at the leading order; the universality at nonzero μ follows once that at $\mu = 0$ is provided [8]. For this reason, except Sec. 3.2 where we discuss the $1/N_c$ correction to the deconfinement temperature, we shall mostly concentrate on the phases related to the chiral and flavor dynamics which presumably depend on μ at the leading order of $1/N_c$ expansion.

[4]The BEC regions in these theories appear in a model-independent way (see the discussion in Sec. 2). This is in contrast to QCD at finite μ_B where the BEC of diquark pairing can appear depending on the details of the models [16, 17]. Throughout this paper, we assume the crossover between the BEC and BCS regions similarly to [7, 18] though our result of the universality of the phase diagrams does not rely on this assumption.

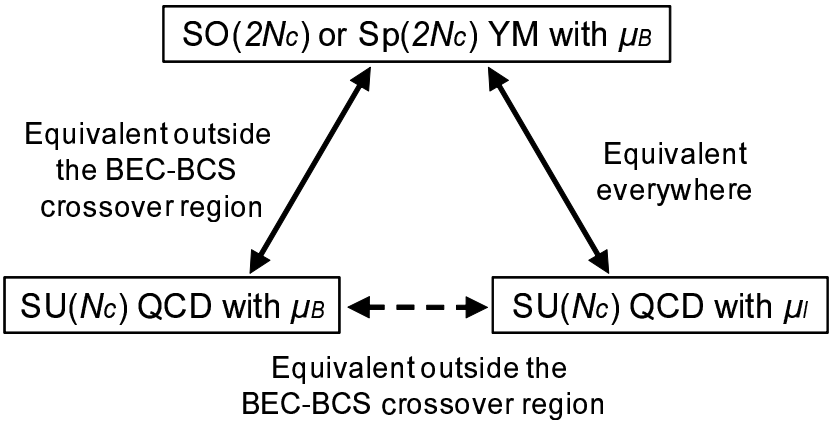

Figure 1: Relations between SU(N_c) QCD at finite μ_B (μ_I) and SO($2N_c$) and Sp($2N_c$) Yang-Mills (YM) theories at finite μ_B. SU(N_c) QCD at finite μ_I can be obtained from SO($2N_c$) or Sp($2N_c$) gauge theory at finite μ_B through the orbifold projection in the whole phase diagram, while QCD at finite μ_B can be obtained outside the BEC-BCS crossover region of these theories. As a result, QCD at finite μ_B is equivalent to QCD at finite μ_I outside the BEC-BCS crossover region of the latter.

fundamental fermions at finite μ_B through an orbifold projection. Here it is this condition, "outside the BEC-BCS region" mentioned above, that U(1) baryon number symmetry of the parent SO($2N_c$) and Sp($2N_c$) gauge theories, which is used for the projection, is not broken spontaneously.

To be precise, the orbifold equivalence has been proven to all orders in the perturbation theory but not nonperturbatively, except certain QCD-like theories containing adjoint scalar or fermion matter at $\mu_B = \mu_I = 0$ [31] and supersymmetric QCD at finite μ_B or μ_I in a holographic setup [37]. In this paper, we provide new evidence for the nonperturbative orbifold equivalence within real QCD and QCD-like theories with fundamental fermions. At sufficiently large chemical potential, nonperturbative observables, such as the superfluid gap and the diquark condensate, can be computed using the controlled weak-coupling calculations owing to the asymptotic freedom. Then we can explicitly compute the $1/N_c$ corrections and demonstrate that the equivalence is not only exact in the large-N_c limit but is well satisfied even for $N_c = 3$. We also apply the idea of the orbifold equivalence to the chiral random matrix theory, a solvable large-N (large volume) matrix model of QCD (for reviews, see [38, 39]). We verify the nonperturbative orbifold equivalence between the random matrix theories of different universality classes by computing the effective potentials in the $N \to \infty$ limit (thermodynamic limit). Our calculations and arguments, though do not constitute a complete proof, provide overwhelming evidence for the nonperturbative equivalence in real QCD at finite chemical potential.

The paper is organized as follows. In Sec. 2, we study the properties of SU(N_c), SO($2N_c$), and Sp($2N_c$) gauge theories at finite chemical potential. In Sec. 3, after a brief review of the orbifold equivalence in the large-N_c QCD, we construct the orbifold projections between QCD and QCD-like theories. We then argue that the phase diagrams of these theories should be universal. Also we compute the $1/N_c$ corrections at asymptotically high

density. In Sec. 4, we construct the orbifold projections between the chiral random matrix theories of the different universality classes. We then explicitly check the nonperturbative orbifold equivalence. Section 5 is devoted to conclusion and discussion.

2. Classification of QCD and QCD-like theories

In sections 2 and 3, we consider the following classes of theories: SU($N_c \geq 3$), SO($2N_c$), and Sp($2N_c$) Yang-Mills theories with N_f fundamental Dirac fermions. For SU(N_c) gauge theory, we consider finite baryon chemical potential μ_B or finite isospin chemical potential μ_I. For SO($2N_c$) and Sp($2N_c$) gauge theories, we consider finite baryon chemical potential μ_B. We can classify these theories by the Dyson index β of the Dirac operator which reflects the number of independent degrees of freedom per matrix element in corresponding chiral random matrix theories, as we will briefly review in Sec. 4: SU(N_c), SO($2N_c$), and Sp($2N_c$) gauge theories correspond to $\beta = 2$, $\beta = 4$, and $\beta = 1$, respectively.

The Lagrangian of the gauge theories in the Euclidean spacetime is given by

$$\mathcal{L}_G = \frac{1}{4g_G^2}\,\mathrm{tr}(F_{\mu\nu}^G)^2 + \sum_{f=1}^{N_f} \bar{\psi}_f^G(\mathcal{D}+m)\psi_f^G, \tag{2.1}$$

where G denotes the gauge group SU(N_c), SO($2N_c$), or Sp($2N_c$) and f denotes the flavor index. $F_{\mu\nu}^G$ is the field strength of each gauge field $A_\mu^G = A_{\mu a}^G T_a^G$ with T_a^G being the generators of each gauge group normalized such that $\mathrm{tr}(T_a^G T_b^G) = (1/2)\delta_{ab}$. The Dirac fermion ψ_f^G belongs to the fundamental representation of the gauge group G,[5] and $m_f = m$ is the degenerate quark mass.[6] The Dirac operator $\mathcal{D}$ is defined as

$$\mathcal{D} = \gamma^\mu D_\mu + \mu\gamma^4, \tag{2.2}$$

for finite quark chemical potential μ, and

$$\mathcal{D} = \gamma^\mu D_\mu + \frac{1}{2}\mu_I\gamma^4\tau^3, \tag{2.3}$$

for finite isospin chemical potential $\mu_I = 2\mu$ when $N_f = 2$.[7] Here $D_\mu = \partial_\mu + iA_\mu^G$ is the color covariant derivative. The SU(2) isospin generators τ_i are normalized such that $\mathrm{tr}(\tau_i\tau_j) = 2\delta_{ij}$. In both cases above, the Dirac operator preserves the chiral symmetry $\{\gamma_5, \mathcal{D}\} = 0$.

In this section, we will investigate the properties (the phase diagram in particular) of each gauge theory. For completeness, we repeat some of arguments on SU(N_c) QCD at finite μ_B [3] and μ_I [7] in the literature. The arguments in this section are independent of N_c, except that we consider $N_c \geq 3$ for SU(N_c) QCD.

[5] For $G = \mathrm{SO}(2N_c)$, it is the $2N_c$-component vector representation.

[6] The degenerate quark mass is not essential in our argument. In order to avoid the sign problem, pairwise m_f is necessary in SU(N_c) QCD at finite μ_I and Sp($2N_c$) gauge theory at finite μ_B, but is not in SO($2N_c$) gauge theory at finite μ_B. See the subsections below.

[7] In this paper, we consider the isospin chemical potential μ_I for $N_f = 2$ unless otherwise stated explicitly. Our argument can be generalized to any even N_f if we define μ_I by regarding $N_f/2$ quarks as "up" with the quark chemical potential μ and $N_f/2$ quarks as "down" with the quark chemical potential $-\mu$.

2.1 QCD: SU($N_c \geq 3$) gauge theory at finite μ_B ($\beta = 2$)

Let us first consider the SU($N_c \geq 3$) gauge theory with fundamental fermions (QCD). In the QCD vacuum ($\mu = 0$), the Dirac operator $\mathcal{D}$ is anti-Hermitian and its eigenvalue $i\lambda_n$ defined by $\mathcal{D}\psi_n = i\lambda_n\psi_n$ is always pure imaginary, $\lambda_n \in \mathbb{R}$. From the chiral symmetry $\{\gamma_5, \mathcal{D}\} = 0$, $-i\lambda_n$ is also the eigenvalue when $\lambda_n \neq 0$ and the fermion determinant $\det(\mathcal{D}+m)$ is always real and nonnegative. This allows us to use the standard Monte-Carlo simulation based on the importance sampling. However, this is no longer true in QCD at finite μ_B. Because λ_n is generally complex and so is the fermion determinant, the standard Monte-Carlo simulation technique fails (the fermion sign problem). In this case, the Dirac operator is written in the form of the complex matrix [see (4.3)], and the Dyson index is $\beta = 2$.

Although present understanding of the QCD phase diagram at intermediate μ_B is largely model-dependent [1], the ground state of QCD at low T and at sufficiently large μ_B is expected to be a color superconductor [3] based on the controlled weak-coupling calculations. At sufficiently large μ_B, the physics near the Fermi surface is described by the weakly interacting quarks due to the asymptotic freedom. The perturbative one-gluon exchange interaction,

$$\mathcal{L}_{\rm OGE} = -G(\bar{\psi}\gamma^\mu T_a^{\rm SU}\psi)^2, \tag{2.4}$$

is dominant at large μ_B with $G > 0$. The color factor of this interaction in the $\psi\psi$-channel is

$$(T_a^{\rm SU})_{\alpha\beta}(T_a^{\rm SU})_{\gamma\delta} = \frac{N_c-1}{N_c}(T_S^{\rm U})_{\alpha\gamma}(T_S^{\rm U})_{\delta\beta} - \frac{N_c+1}{N_c}(T_A^{\rm SU})_{\alpha\gamma}(T_A^{\rm SU})_{\delta\beta}, \tag{2.5}$$

where $T_S^{\rm U}$ and $T_A^{\rm SU}$ are symmetric and antisymmetric $N_c \times N_c$ Hermitian matrices. This is attractive in the color antisymmetric channel. According to the Bardeen-Cooper-Schrieffer (BCS) mechanism, any infinitesimally small attractive interaction between quarks leads to the condensation of quark-quark pairs, the diquark condensate. Because the positive parity state is favored by instanton effects [40, 41], the pairing in the spin-parity 0^+ channel is the most favorable energetically. Considering the Pauli principle, the condensate must be flavor antisymmetric. Therefore, the condensate $\langle\psi^T C\gamma_5 T_A \tau_{A'}\psi\rangle$ is formed at large μ_B, where both A and A' denote antisymmetric representations. Since the diquark condensate breaks SU(N_c) color symmetry, this is called the color superconductivity [3].

2.2 QCD: SU($N_c \geq 3$) gauge theory at finite μ_I ($\beta = 2$)

Now we turn to QCD at finite μ_I and $\mu_B = 0$ (see [7] for details). Due to the property $\tau_1\tau_3\tau_1 = -\tau_3$, the Dirac operator (2.3) satisfies

$$\tau_1\gamma_5\mathcal{D}\gamma_5\tau_1 = \mathcal{D}^\dagger. \tag{2.6}$$

From this relation and the chiral symmetry $\{\gamma_5, \mathcal{D}\} = 0$, if we take an eigenvalue $i\lambda_n$ of the Dirac operator (2.3), eigenvalues appear in quartet $(i\lambda_n, -i\lambda_n, i\lambda_n^*, -i\lambda_n^*)$. Therefore, one finds that $\det[\mathcal{D}(\mu) + m] \geq 0$ and the standard Monte-Carlo simulation technique can be used at finite μ_I.

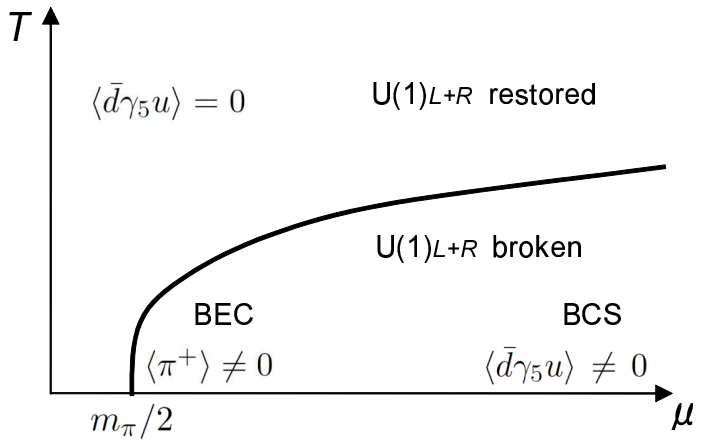

Figure 2: Phase diagram of QCD at finite $\mu_I = 2\mu$.

When $m = \mu_I = 0$, the Lagrangian has $\mathrm{SU}(2)_L \times \mathrm{SU}(2)_R$ symmetry. If the degenerate quark mass m is turned on, the symmetry is explicitly broken to $\mathrm{SU}(2)_{L+R}$. The isospin chemical potential μ_I further breaks $\mathrm{SU}(2)_{L+R}$ down to $\mathrm{U}(1)_{L+R}$. Note that this symmetry is different from $\mathrm{U}(1)_B$.

Let us consider the zero-temperature ground state at small μ_I and sufficiently large μ_I where the theory is analytically controllable. Unlike the phase structure of QCD at finite μ_B, that of QCD at finite μ_I (with degenerate quark mass) is rather well understood because of the absence of the sign problem and the constraints from the rigorous QCD inequalities [42, 43, 44, 45] [4, 5], where both properties follow from the relation (2.6). The phase diagram in the T-μ plane is summarized in Fig. 2. For small μ_I below the ρ meson mass m_ρ, we can concentrate on the pions at low-energy. When $\mu_I < m_\pi$, no particles can be excited so that the ground state is the same as the QCD vacuum at $\mu_I = 0$. On the other hand, when $\mu_I > m_\pi$, it is favorable to excite π^+ whose excitation energy is $m_\pi - \mu_I < 0$; the ground state turns into the Bose-Einstein condensation (BEC) phase, $\langle \pi^+\rangle \neq 0$, where $\mathrm{U}(1)_{L+R}$ is spontaneously broken down to $\mathbb{Z}_2$.

At sufficiently large μ_I, on the other hand, $\mathrm{U}(1)_{L+R}$ symmetry is spontaneously broken by the BCS-type diquark pairing. The color factor of the one-gluon exchange interaction in the $\bar{\psi}\psi$-channel is

$$(T_a^{\mathrm{SU}})_{\alpha\beta}(T_a^{\mathrm{SU}})_{\gamma\delta} = \frac{N_c^2-1}{2N_c^2}(\mathbf{1})^{N_c}_{\alpha\delta}(\mathbf{1})^{N_c}_{\gamma\beta} - \frac{1}{N_c}(T_a^{\mathrm{SU}})_{\alpha\delta}(T_a^{\mathrm{SU}})_{\gamma\beta}, \tag{2.7}$$

which is attractive in the color-singlet channel. The spin-parity 0^- channel is favored by the instanton effects, and the condensate must be flavor antisymmetric from the Pauli principle, $\langle \bar{d}\gamma_5 u\rangle \neq 0$. This is consistent with the requirement from the QCD inequality [7]. Note that, although the mechanism leading to the pairing is similar to the color superconductivity in QCD at large μ_B, this condensate has different quantum numbers and does not break $\mathrm{SU}(N_c)$ color symmetry.

Since the BCS pairing $\langle \bar{d}\gamma_5 u\rangle \neq 0$ at large μ_I has the same quantum numbers and breaks the same $\mathrm{U}(1)_{L+R}$ symmetry as the BEC $\langle \pi^+\rangle \neq 0$ at small μ_I, it is natural to

expect that the BEC and BCS regions are continuously connected without any phase transition (the BEC-BCS crossover). At sufficiently high T, the condensate melts away and $\mathrm{U}(1)_{L+R}$ symmetry recovers. The critical temperature T_c vanishes at $\mu = m_\pi/2$ and is expected to be an increasing function of μ in both BEC and BCS regions.

2.3 $\mathbf{SO}(2N_c)$ gauge theory at finite μ_B ($\beta = 4$)

We next consider $\mathrm{SO}(2N_c)$ gauge theory at finite μ_B. From the property $(A_\mu^{\mathrm{SO}})^* = -A_\mu^{\mathrm{SO}}$, one has the relation:

$$C\gamma_5 \mathcal{D} C\gamma_5 = \mathcal{D}^*, \quad \text{or} \quad [\mathcal{D}, C\gamma_5 K] = 0, \tag{2.8}$$

where C is the charge conjugation matrix satisfying $C^2 = 1$ and $C\gamma^\mu C = -\gamma^{\mu *}$ with all γ matrices being Hermitian, and K is the complex conjugation operator. The Dirac operator can be written in the form of quaternion real matrix [see (4.5)] and the Dyson index is $\beta = 4$, the same universality class as $\mathrm{SU}(N_c)$ gauge theory with adjoint fermions [5] (see also [46]). From (2.8) and the chiral symmetry $\{\gamma_5, \mathcal{D}\} = 0$, if $i\lambda_n$ is one of the eigenvalues of $\mathcal{D}$, eigenvalues appear in quartet $(i\lambda_n, -i\lambda_n, i\lambda_n^*, -i\lambda_n^*)$. Note that, when λ_n is real or pure imaginary, this quartet reduces to two sets of doublets $(i\lambda_n, -i\lambda_n)$ with their eigenvectors being linearly independent from the anti-unitary symmetry (2.8) [47]. Therefore, $\det[\mathcal{D}(\mu) + m] \geq 0$ and the standard Monte-Carlo simulation technique is available at finite μ_B [35, 36].

When $m = \mu_B = 0$, the Lagrangian (2.1) has the $\mathrm{SU}(N_f)_L \times \mathrm{SU}(N_f)_R \times \mathrm{U}(1)_B \times \mathrm{U}(1)_A$ symmetry at the classical level at first sight. However, chiral symmetry of the theory is enhanced to $\mathrm{U}(2N_f)$ owing to the anti-unitary symmetry (2.8) [48, 49]. At the quantum level, $\mathrm{U}(1)_A \subset \mathrm{U}(2N_f)$ is explicitly broken by the axial anomaly and $\mathrm{SU}(2N_f)$ symmetry remains. One can actually rewrite the fermionic part of the Lagrangian (2.1) manifestly invariant under $\mathrm{SU}(2N_f)$ using the new variable $\Psi = (\psi_L, \sigma_2 \psi_R^*)^T$:

$$\mathcal{L}_{\mathrm{f}} = i\Psi^\dagger \sigma_\mu D_\mu \Psi, \tag{2.9}$$

where $\sigma_\mu = (-i, \sigma_k)$ with the Pauli matrices σ_k. The chiral symmetry $\mathrm{SU}(2N_f)$ is spontaneously broken down to $\mathrm{SO}(2N_f)$ by the formation of the chiral condensate $\langle \bar{\psi}\psi \rangle$, leading to the $2N_f^2 + N_f - 1$ Nambu-Goldstone (NG) bosons living on the coset space $\mathrm{SU}(2N_f)/\mathrm{SO}(2N_f)$. In contrast to real QCD, there are not only $\mathrm{U}(1)_B$ neutral NG modes with the quantum numbers $\Pi_a = \bar{\psi}\gamma_5 P_a \psi$ (just like the usual pions), but also $\mathrm{U}(1)_B$ charged NG modes with the quantum numbers $\Sigma_S = \psi^T C\gamma_5 Q_S \psi$ and $\Sigma_S^\dagger = \psi^\dagger C\gamma_5 Q_S \psi^*$. Here P_a are traceless and Hermitian $N_f \times N_f$ matrices, $P_a = P_a^\dagger$ $(a = 1, 2, \cdots, N_f^2 - 1)$, and Q_S are symmetric $N_f \times N_f$ matrices, $Q_S^T = Q_S$ $(S = 1, 2, \cdots, N_f(N_f+1)/2)$, in the flavor space. The chiral perturbation theory describing these NG modes for small $\mu \lesssim m_\rho/2$ is exactly the same as that of $\mathrm{SU}(N_c)$ gauge theory with adjoint fermions at finite μ_B considered in [5], because their symmetry breaking patterns are the same: the low-energy physics is dictated by the Dyson index $\beta = 4$.

Let us consider the phase diagram of this theory. For $m_\pi/2 < \mu \lesssim m_\rho/2$ at $T = 0$, it is energetically favorable for the $\mathrm{U}(1)_B$ charged NG modes Σ_S with the excitation energy

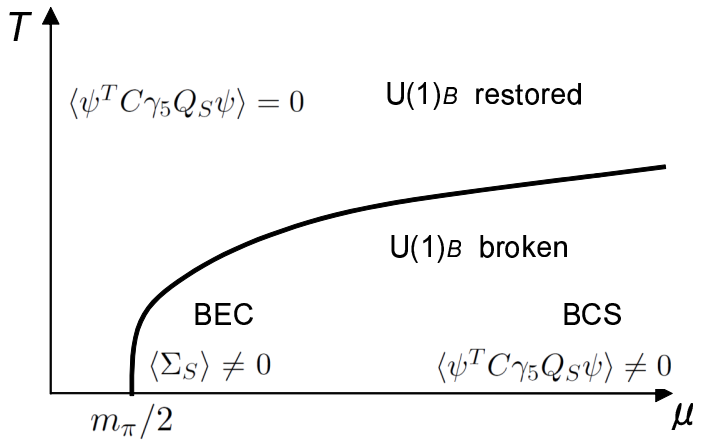

Figure 3: Phase diagram of $\mathrm{SO}(2N_c)$ gauge theory at finite μ_B.

$m_\pi - 2\mu < 0$ to form the BEC, $\langle\Sigma_S\rangle \neq 0$. On the other hand, at sufficiently large μ, the one-gluon exchange interaction in the $\psi\psi$-channel is attractive in the color symmetric channel, leading to the condensation of the diquark pairing. Due to the Pauli principle, the BCS diquark pairing must be flavor symmetric, and takes the form $\langle\psi^T C\gamma_5 Q_S\psi\rangle \neq 0$. This BCS pairing has the same quantum numbers and breaks the same symmetry as the BEC at small μ_B, and it is plausible that no phase transition occurs between the BEC and BCS regions. The phase diagram of this theory is similar to that of QCD at finite μ_I, as shown in Fig. 3.

2.4 $\mathbf{Sp}(2N_c)$ gauge theory at finite μ_B ($\beta = 1$)

We turn to $\mathrm{Sp}(2N_c)$ gauge theory at finite μ_B. From the property $J_c A_\mu^{\mathrm{Sp}} J_c = (A_\mu^{\mathrm{Sp}})^*$ with

$$J_c = -i\sigma_2 \otimes \mathbf{1}_{N_c} \tag{2.10}$$

one has the relation:

$$J_c C\gamma_5 \mathcal{D} C\gamma_5 J_c = -\mathcal{D}^*, \quad \text{or} \quad [\mathcal{D}, iJ_c C\gamma_5 K] = 0. \tag{2.11}$$

The Dirac operator can be written in the form of real matrix [see (4.4)], and the Dyson index is $\beta = 1$, the same universality class as two-color QCD [4, 5] (see also [46]). One then finds that $\det[\mathcal{D}(\mu) + m] \geq 0$ for even N_f. Note here that even N_f is necessary for the positivity unlike $\mathrm{SO}(2N_c)$ gauge theory, because the quartet structure of eigenvalues $(i\lambda_n, -i\lambda_n, i\lambda_n^*, -i\lambda_n^*)$ reduces to one set of doublet $(i\lambda_n, -i\lambda_n)$ when λ_n is real or pure imaginary [47].

When $m = \mu_B = 0$, because of the anti-unitary symmetry (2.11), chiral symmetry of the theory is enhanced to $\mathrm{SU}(2N_f)$ [48, 49]. This can be seen by rewriting the fermionic part of the Lagrangian (2.1) using the new variable $\Psi = (\psi_L, \sigma_2\tau_2\psi_R^*)^T$:

$$\mathcal{L}_{\mathrm{f}} = i\Psi^\dagger \sigma_\mu D_\mu \Psi, \tag{2.12}$$

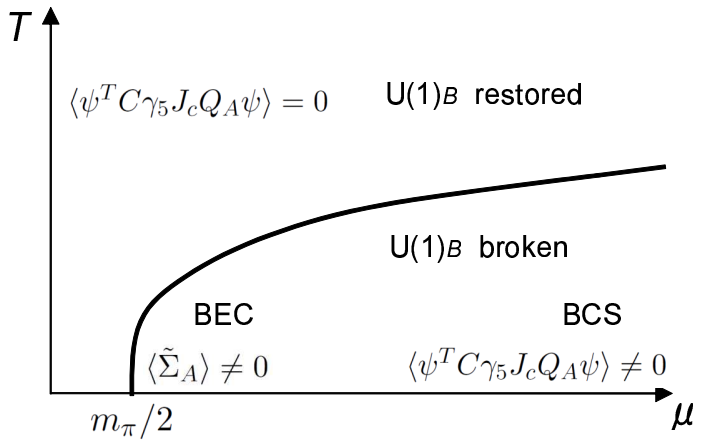

Figure 4: Phase diagram of $\mathrm{Sp}(2N_c)$ gauge theory at finite μ_B.

which is manifestly invariant under $\mathrm{SU}(2N_f)$. The chiral symmetry is spontaneously broken down to $\mathrm{Sp}(2N_f)$ by the formation of the chiral condensate $\langle\bar{\psi}\psi\rangle$, giving rise to $2N_f^2 - N_f - 1$ NG bosons parametrized by the coset space $\mathrm{SU}(2N_f)/\mathrm{Sp}(2N_f)$. There are both $\mathrm{U}(1)_B$ neutral NG modes with the quantum numbers $\Pi_a = \bar{\psi}\gamma_5 P_a \psi$ and $\mathrm{U}(1)_B$ charged NG modes with the quantum numbers $\tilde{\Sigma}_A = \psi^T C\gamma_5 J_c Q_A \psi$ and $\tilde{\Sigma}_A^\dagger = \psi^\dagger C\gamma_5 J_c Q_A \psi^*$. Here P_a are traceless and Hermitian $N_f \times N_f$ matrices, $P_a = P_a^\dagger$ $(a = 1, 2, \cdots, N_f^2 - 1)$, and Q_A are antisymmetric $N_f \times N_f$ matrices, $Q_A^T = -Q_A$ $(A = 1, 2, \cdots, N_f(N_f-1)/2)$, in the flavor space. The chiral perturbation theory for small $\mu \lesssim m_\rho/2$ is the same as that of two-color QCD at finite μ_B [4, 5] because of the same symmetry breaking pattern dictated by the Dyson index $\beta = 1$.

For $m_\pi/2 < \mu \lesssim m_\rho/2$ at $T = 0$, the $\mathrm{U}(1)_B$ charged NG modes form the BEC, $\langle\tilde{\Sigma}_A\rangle \neq 0$. At sufficiently large μ, the one-gluon exchange interaction in the $\psi\psi$-channel is attractive in the color antisymmetric channel and induces the condensation of the color and flavor antisymmetric BCS diquark pairing $\langle\psi^T C\gamma_5 J_c Q_A \psi\rangle \neq 0$. Note that the diquark condensate has the different quantum numbers from the ones in $\mathrm{SO}(2N_c)$ gauge theory. The BEC-BCS crossover of the diquark pairing is expected in this theory again, as depicted in Fig. 4.

2.5 Brief summary

Before proceeding, we summarize the results in this section.

1. QCD at finite μ_B (or μ_I), $\mathrm{SO}(2N_c)$ gauge theory at finite μ_B, and $\mathrm{Sp}(2N_c)$ gauge theory at finite μ_B belong to the different universality classes denoted by the Dyson indices $\beta = 2$, $\beta = 4$, and $\beta = 1$, respectively.

2. QCD at finite μ_I and $\mathrm{SO}(2N_c)$ and $\mathrm{Sp}(2N_c)$ gauge theories at finite μ_B have *no* fermion sign problem and exhibit the BEC-BCS crossover phenomena in the phase diagrams.

Apparently, the phase diagrams of the three theories, QCD at finite μ_I, SO($2N_c$) gauge theory at finite μ_B, and Sp($2N_c$) gauge theory at finite μ_B, resemble each other qualitatively. In the next section, we will argue that these phase diagrams should be completely identical in the large-N_c limit, including the chiral phase transition (not shown in figures). Also we will show that the phase diagram of QCD at finite μ_B should also be identical to them outside the BEC-BCS crossover regions.

3. Orbifold equivalence in the large-N_c QCD and QCD-like theories

In this section, we first briefly recapitulate the basic idea of the orbifold equivalence in large-N_c gauge theories. We then construct orbifold projection from SO($2N_c$) or Sp($2N_c$) gauge theory at finite μ_B to SU(N_c) QCD at finite μ_B or μ_I. The relations between these theories via orbifold projections are summarized in Fig. 1.[8]

3.1 Perturbative orbifold equivalence in pure gauge theories

The main idea of the orbifold projection is as follows: we identify a discrete subgroup of the symmetry group of the "parent" theory, that is the SO($2N_c$) or Sp($2N_c$) gauge theory in our case. We then eliminate all of the degrees of freedom in the parent theory which are not invariant under the discrete symmetry. This gives the "daughter" theory, which will turn out to be the SU(N_c) gauge theory. We use a $\mathbb{Z}_2$ subgroup of the original SO($2N_c$) or Sp($2N_c$) gauge theory for the orbifold projection. In the large-N_c limit for fixed N_f (the 't Hooft limit), correlation functions of operators $\mathcal{O}_i^{(p)}$ in the parent theory invariant under the projection symmetry (which we call the "neutral operators"), and those of the operators $\mathcal{O}_i^{(d)}$ in the daughter theory made up of the projected fields, coincide to all orders in the perturbation theory [27],

$$\langle \mathcal{O}_1^{(p)} \mathcal{O}_2^{(p)} \cdots \rangle_p = \langle \mathcal{O}_1^{(d)} \mathcal{O}_2^{(d)} \cdots \rangle_d. \tag{3.1}$$

In this sense, the parent theory and the daughter theory are equivalent. Especially, magnitudes of neutral order parameters characterizing the phases should be exactly the same.

Let us first consider the orbifold projection of the pure SO($2N_c$) gauge theory. (For an earlier work of the orbifold projection from SO($2N_c$) to SU(N_c), see [34].) For the "projection," we use $\mathbb{Z}_4$ subgroup of SO($2N_c$) generated by J_c defined in (2.10). J_c satisfies the condition,

$$\mathrm{tr}(J_c^n) = 0, \tag{3.2}$$

when J_c^n does not belong to the center of SO($2N_c$), i.e., $J_c^n \neq \pm \mathbf{1}_{2N_c}$. This condition is called the "regularity condition," which is utilized in the perturbative proof of the orbifold

[8] We can also construct the orbifold projections (not shown in Fig. 1) from SO($2N_c$) gauge theory with adjoint fermions at finite μ_B to SU(N_c) QCD with adjoint fermions at finite μ_B and to SU(N_c) QCD with antisymmetric fermions at finite μ_I, generalizing the argument of [31] to the case with finite chemical potential. The resultant equivalence between SU(N_c) QCD with adjoint fermions and SU(N_c) QCD with antisymmetric fermions is a generalization of the *orientifold equivalence* [50] to finite chemical potential.

equivalence. The transformation of $A_\mu^{\rm SO}$ induced by J_c is written as

$$(A_\mu^{\rm SO})_{ij} \to (J_c)_{ii'}(A_\mu^{\rm SO})_{i'j'}(J_c)^{-1}_{j'j}, \tag{3.3}$$

which constitutes $\mathbb{Z}_2$ subgroup of the gauge group. We define the projection condition for the gauge field $A_\mu^{\rm SO}$ to be invariant under the $\mathbb{Z}_2$ subgroup:

$$(A_\mu^{\rm SO})_{ij} = (J_c)_{ii'}(A_\mu^{\rm SO})_{i'j'}(J_c)^{-1}_{j'j}. \tag{3.4}$$

The gauge field $A_\mu^{\rm SO}$ satisfying this condition can be obtained by using the projector $\mathcal{P}$ defined as

$$\mathcal{P}(A_\mu^{\rm SO}) = \frac{1}{4}\sum_{n=0}^{3} J_c^n A_\mu^{\rm SO} J_c^{-n} = \frac{1}{2}\left(A_\mu^{\rm SO} + J_c A_\mu^{\rm SO} J_c^{-1}\right), \tag{3.5}$$

where 4 is the number of elements of $\mathbb{Z}_4$.

Remembering the property $(A_\mu^{\rm SO})^* = -A_\mu^{\rm SO}$, the gauge field $A_\mu^{\rm SO}$ can be written as

$$A_\mu^{\rm SO} = i\begin{pmatrix} A_\mu^A + B_\mu^A & C_\mu^A - D_\mu^S \\ C_\mu^A + D_\mu^S & A_\mu^A - B_\mu^A \end{pmatrix}, \tag{3.6}$$

where the fields A_μ^A, B_μ^A, and C_μ^A (D_μ^S) are $N_c \times N_c$ anti-symmetric (symmetric) matrices. Under the $\mathbb{Z}_2$ symmetry, A_μ^A, D_μ^S are even while B_μ^A, C_μ^A are odd, so the orbifold projection sets $B_\mu^A = C_\mu^A = 0$. Hence we have

$$A_\mu^{\rm proj} = i\begin{pmatrix} A_\mu^A & -D_\mu^S \\ D_\mu^S & A_\mu^A \end{pmatrix}. \tag{3.7}$$

If one performs a unitary transformation in the color space using the matrix

$$P_c = \frac{1}{\sqrt{2}}\begin{pmatrix} \mathbf{1}_{N_c} & i\mathbf{1}_{N_c} \\ \mathbf{1}_{N_c} & -i\mathbf{1}_{N_c} \end{pmatrix}, \tag{3.8}$$

$A_\mu^{\rm proj}$ can be expressed by the U(N_c) gauge field $A_\mu^{\rm U} \equiv D_\mu^S + iA_\mu^A$ as

$$P_c A_\mu^{\rm proj} P_c^{-1} = \begin{pmatrix} -(A_\mu^{\rm U})^T & 0 \\ 0 & A_\mu^{\rm U} \end{pmatrix}. \tag{3.9}$$

The top left component is the charge conjugation of the bottom right component, $-(A_\mu^{\rm U})^T = (A_\mu^{\rm U})^C$. At large N_c, we can neglect the difference between U(N_c) and SU(N_c) up to $1/N_c^2$ corrections, $A^{\rm U} \simeq A^{\rm SU}$.[9] Therefore, the action of the SO($2N_c$) gauge theory,

$$\mathcal{L}_{\rm SO} = \frac{1}{4g_{\rm SO}^2}\,{\rm tr}(F_{\mu\nu}^{\rm SO})^2, \tag{3.10}$$

[9]Notice the chemical potential is introduced as a boundary condition for the U(1) part of the gauge field at infinity. However it is not easy to impose an appropriate boundary condition at infinity in lattice simulations; although the integration region of the path integral must be limited so that it does not alter the boundary condition (in particular constant shift of the gauge field, $A_\mu \to A_\mu + C$, is forbidden), all field configurations, including constant shift, are summed over in actual lattice simulations. Because of this lattice artifact, μ-dependence disappears in U(N_c) gauge theory [51]. In SU(N_c) gauge theory, this problem does not arise.

is projected to that of the SU(N_c) gauge theory,

$$\mathcal{L}_{\rm proj} = \frac{2}{4g^2_{\rm SU}} \,{\rm tr}(F^{\rm SU}_{\mu\nu})^2, \tag{3.11}$$

where $F^{\rm SU}_{\mu\nu}$ is the field strength of the SU(N_c) gauge field $A^{\rm SU}_\mu$. In this way, SU(N_c) gauge theory is obtained from SO($2N_c$) gauge theory via the *orbifold projection*.

We can similarly define the orbifold projection of the Sp($2N_c$) gauge theory. The symplectic algebra Sp($2N_c$) formed by $2N_c \times 2N_c$ Hermitian matrices satisfies

$$J_c A^{\rm Sp} + (A^{\rm Sp})^T J_c = 0, \tag{3.12}$$

and can be written as

$$A^{\rm Sp}_\mu = \begin{pmatrix} iA^A_\mu + B^S_\mu & C^S_\mu - iD^S_\mu \\ C^S_\mu + iD^S_\mu & iA^A_\mu - B^S_\mu \end{pmatrix}. \tag{3.13}$$

Here the fields A^A_μ (B^S_μ, C^S_μ, and D^S_μ) are $N_c \times N_c$ anti-symmetric (symmetric) matrices. If we choose the same projection condition for $A^{\rm Sp}$ as (3.4),

$$A^{\rm Sp}_\mu = J_c A^{\rm Sp}_\mu J_c^{-1}. \tag{3.14}$$

one obtains $B^S_\mu = C^S_\mu = 0$. This gives the SU(N_c) gauge theory again.

The mapping rule of the large-N_c orbifold equivalence is as follows: if we equate the parent action with *twice* the daughter action for the $\mathbb{Z}_2$ orbifold projection [31, 32],

$$\mathcal{L}_{\rm SO(Sp)} \to 2\mathcal{L}_{\rm SU}, \tag{3.15}$$

these two theories are equivalent in the sense that (3.1) holds within the neutral sectors i.e., the correlation functions of the neutral operators. The reason of this factor 2 will be clarified below [see (3.21)]. From the recipe (3.15), we must take the action of the daughter SU(N_c) gauge theory as

$$\mathcal{L}_{\rm SU} = \frac{1}{4g^2_{\rm SU}} \,{\rm tr}(F^{\rm SU}_{\mu\nu})^2, \tag{3.16}$$

with the coupling constant $g_{\rm SU}$ satisfying

$$g_{\rm SO(Sp)} = g_{\rm SU}. \tag{3.17}$$

Let us give a schematic of the proof of the orbifold equivalence to all orders in the perturbation theory following Bershadsky and Johansen [27]. This can be easily generalized to the cases with the fundamental fermions [35], as we will see in the next subsection. We assume that the gauge fixing condition is consistent with the projection – the ghosts are related by the projection, and all propagators in two theory takes the same form up to the color factors.

As a pedagogical demonstration, consider a vacuum planar diagram of the SO($2N_c$) or Sp($2N_c$) gauge theory in Fig. 5. In order to obtain the SU(N_c) diagram from the SO($2N_c$)

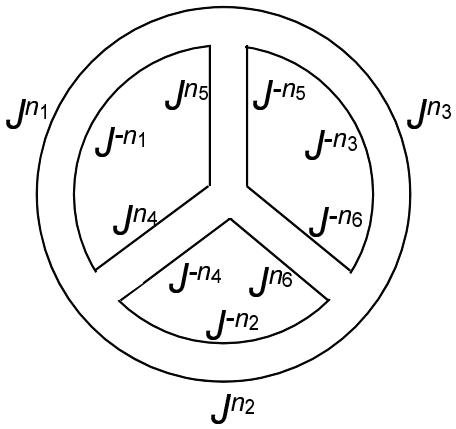

Figure 5: A vacuum planar diagram in the double-line notation.

or $\mathrm{Sp}(2N_c)$ diagram, we insert the projector $\mathcal{P}$ to each propagator. Because the 't Hooft couplings are taken to be the same and the propagators are the same up to color factors, the only difference, if exists, comes from the contractions of color indices. Remembering (3.5), the additional kinematic factor multiplied by the $\mathrm{SU}(N_c)$ diagram is

$$\sum_{n_i=0,1} \left(\frac{1}{2}\right)^{N_P} \cdot \mathrm{tr}(J^{-n_1} J^{n_4} J^{n_5}) \cdot \mathrm{tr}(J^{-n_2} J^{-n_4} J^{n_6}) \cdot \mathrm{tr}(J^{-n_3} J^{-n_5} J^{-n_6}) \cdot \mathrm{tr}(J^{n_1} J^{n_2} J^{n_3}), \tag{3.18}$$

where $J = -i\sigma_2$ is a 2×2 matrix and the factor $(1/2)^{N_P}$ comes from the projectors with $N_P = 6$ being the number of propagators. Because of the regularity condition (3.2), it is nonvanishing only when

$$J^{-n_1} J^{n_4} J^{n_5} = \pm \mathbf{1}_2, \quad J^{-n_2} J^{-n_4} J^{n_6} = \pm \mathbf{1}_2, \quad J^{-n_3} J^{-n_5} J^{-n_6} = \pm \mathbf{1}_2, \quad J^{n_1} J^{n_2} J^{n_3} = \pm \mathbf{1}_2. \tag{3.19}$$

The last condition follows from the others, and hence, there are $N_L - 1 = 3$ independent constraints, where $N_L = 4$ is the number of color index loops. In (3.18) the combinations of $n_i = 0, 1$ for all $N_P = 6$ propagators under the $N_L - 1 = 3$ constraints give a factor of 2^{6-3}, traces over color indices give 2^4, and thus, the total factor is

$$2^{-6} \cdot 2^{6-3} \cdot 2^4 = 2. \tag{3.20}$$

Generally, for any given planar vacuum diagram with N_P propagators and N_L loops, the projectors give a factor of $(1/2)^{N_P}$, the combinations of $n_i = 0, 1$ $(i = 1, 2, \cdots, N_P)$ under the $N_L - 1$ constraints give $2^{N_P - (N_L - 1)}$, and the traces over color indices give 2^{N_L}. Therefore, the total factor is always the same:

$$2^{-N_P} \cdot 2^{N_P - (N_L - 1)} \cdot 2^{N_L} = 2. \tag{3.21}$$

This factor 2 reflects the fact that the number of degrees of freedom in the parent theory is twice larger than that in the daughter theory. Hence the vacuum energy per degree of

freedom is identical between these theories. This is why the recipe (3.15) is necessary to match the degrees of freedom between the parent and daughter theories. However, this argument does not hold for nonplanar diagrams. Actually, one can check that the number of independent constraints is no longer $N_L - 1$, and the kinematic factor is different from 2 counted in (3.21) [27]. This is why we need to take the large-N_c limit to suppress the nonplanar diagrams. We can repeat the same argument to any correlation functions of neutral operators (gauge-invariant operators in this case) in any dimension and any gauge group.

Note that this equivalence holds as long as the projection symmetry, $\mathbb{Z}_2$ subgroup of $\mathrm{SO}(2N_c) \times \mathrm{U}(1)_B$ or $\mathrm{Sp}(2N_c) \times \mathrm{U}(1)_B$, is not broken spontaneously [32]. We will come to this issue in more detail in Sec. 3.3.

3.2 Perturbative orbifold equivalence with fermions

In this subsection, we further include the fermions and define the orbifold projections from $\mathrm{SO}(2N_c)$ and $\mathrm{Sp}(2N_c)$ gauge theories to $\mathrm{SU}(N_c)$ gauge theory at finite μ_B or μ_I.[10]

In order to obtain fermions at finite μ_B, we use $\mathbb{Z}_4$ subgroup of $\mathrm{SO}(2N_c)$ or $\mathrm{Sp}(2N_c)$ gauge group generated by J_c and $\mathbb{Z}_4$ subgroup of $\mathrm{U}(1)_B$ generated by $\omega = e^{i\pi/2}$. We choose the projection condition as

$$\psi_a^{\mathrm{SO(Sp)}} = \omega (J_c)_{aa'} \psi_{a'}^{\mathrm{SO(Sp)}}, \tag{3.22}$$

which generates $\mathbb{Z}_2$ subgroup of $\mathrm{SO}(2N_c) \times \mathrm{U}(1)_B$ or $\mathrm{Sp}(2N_c) \times \mathrm{U}(1)_B$. The color $2N_c$-component fundamental fermion is decomposed into two N_c-component fields,

$$\psi^{\mathrm{SO(Sp)}} = \begin{pmatrix} \psi_a \\ \psi_b \end{pmatrix}, \tag{3.23}$$

with a and b being the color indices. Performing the unitary transformation P_c defined in (3.8), we have

$$P_c \psi^{\mathrm{SO(Sp)}} = \begin{pmatrix} \psi_+ \\ \psi_- \end{pmatrix}, \tag{3.24}$$

where $\psi_\pm \equiv (\psi_a \pm i\psi_b)/\sqrt{2}$. The fermions ψ_+ and ψ_-, which couple to $(A_\mu^{\mathrm{SU}})^C$ and A_μ^{SU} from (3.9), transform as antifundamental and fundamental representations under $\mathrm{SU}(N_c)$, respectively. After the projection (3.22), only the fermion ψ_- survives. Taking into account the relation (3.15), the action of the daughter theory is given by

$$\mathcal{L}_{\mathrm{SU}} = \frac{1}{4g_{\mathrm{SU}}^2} \mathrm{tr}(F_{\mu\nu}^{\mathrm{SU}})^2 + \sum_{f=1}^{N_f} \bar{\psi}_f^{\mathrm{SU}} \left(\gamma^\mu D_\mu + m + \mu\gamma^4 \right) \psi_f^{\mathrm{SU}}, \tag{3.25}$$

[10] The orbifold projection can be generalized to the case with both finite μ_B and finite μ_I. More generally, one can construct the orbifold projection in the system where each flavor has different chemical potential μ_f $(f = 1, 2, \cdots, N_f)$.

where $\psi_a^{\rm SU} = \sqrt{2}\psi_-$, $D_\mu = \partial_\mu + iA_\mu^{\rm SU}$. This theory is QCD at finite baryon chemical potential $\mu_B = N_c\mu$.

On the other hand, in order to obtain fermions at finite μ_I for even N_f, we use $J_c \in {\rm SO}(2N_c)$ [or $J_c \in {\rm Sp}(2N_c)$] and $J_i \in {\rm SU}(2)_{\rm isospin}$ defined by

$$J_i = -i\sigma_2 \otimes 1_{N_f/2}. \tag{3.26}$$

We choose the projection condition to be

$$(J_c)_{aa'}\psi_{a'f'}^{\rm SO(Sp)}(J_i^{-1})_{f'f} = \psi_{af}^{\rm SO(Sp)}. \tag{3.27}$$

The flavor N_f-component fundamental fermion is decomposed into two $(N_f/2)$-component fields,

$$\psi^{\rm SO(Sp)} = (\psi_f \ \psi_g), \tag{3.28}$$

with f and g being the flavor indices. If we define $\varphi_\pm = (\psi_\pm^f \mp i\psi_\pm^g)/\sqrt{2}$ and $\xi_\pm = (\psi_\pm^f \pm i\psi_\pm^g)/\sqrt{2}$, the fermions $\varphi_\pm$ survive but $\xi_\pm$ disappear after the projection (3.27). Because $\varphi_\pm$ couple to $(A_\mu^{\rm SU})^C$ and $A_\mu^{\rm SU}$ respectively, the action of the daughter theory is expressed as

$$\mathcal{L}_{\rm SU} = \frac{1}{4g_{\rm SU}^2}\,{\rm tr}(F_{\mu\nu}^{\rm SU})^2 + \sum_\pm \bar\psi_\pm^{\rm SU}\left(\gamma^\mu D_\mu + m \pm \mu\gamma^4\right)\psi_\pm^{\rm SU}, \tag{3.29}$$

where $\psi_+^{\rm SU} = \sqrt{2}\varphi_-$ and $\psi_-^{\rm SU} = \sqrt{2}\varphi_+^C$. This theory, in which "$\pm$" can be regarded as the isospin indices, has the isospin chemical potential $\mu_I = 2\mu$.

Given the orbifold projections, we now prove the orbifold equivalence of the gauge theories with fermions at finite chemical potential. Let us consider a diagram (a correlation function or an observable) in ${\rm SO}(2N_c)$ or ${\rm Sp}(2N_c)$ gauge theory which have quark loop(s). Here we write both color and flavor index lines for each quark line since the contractions of flavor index loops also give kinematical factors.

We first look into the case with finite μ_I. Because the matrix J_c multiplied from the right in (3.4) is just replaced by J_i in (3.27), we can repeat the proof for the pure gauge theory straightforwardly. For a diagram with N_P propagators and $N_L^{(c)}$ color ($N_L^{(f)}$ flavor) index loops, we count additional kinematical factors originating from contractions of both colors and flavors that are multiplied by the parent ${\rm SU}(N_c)$ diagram. The projectors for the propagators give a factor of $(1/2)^{N_P}$, the combinations of $n_i = 0, 1$ $(i = 1, 2, \cdots, N_P)$ under the $N_L^{(c)} + N_L^{(f)} - 1$ constraints give $2^{N_P-(N_L^{(c)}+N_L^{(f)}-1)}$, and the traces over color and flavor indices give $2^{N_L^{(c)}}$ and $2^{N_L^{(f)}}$ respectively. Therefore, the total factor is

$$2^{-N_P}\cdot 2^{N_P-(N_L^{(c)}+N_L^{(f)}-1)}\cdot 2^{N_L^{(c)}}\cdot 2^{N_L^{(f)}} = 2, \tag{3.30}$$

for any number of quark loops $N_L^{(f)}$.

On the other hand, this argument is not applicable to the case with finite μ_B since the structure of the projection condition (3.22) is different from (3.4) and (3.27). However we can still justify the orbifold equivalence as long as the number of quark loop is one.

Consider a diagram with N_P propagators and $N_L^{(c)}$ color index loop and one fermion index loop. The fermion index loop gives no condition for J^{n_i} in Eq. (3.19), and the number of the constraints for $n_i = 0, 1$ $(i = 1, 2, \cdots, N_P)$ is $N_L^{(c)}$. Then one again concludes that the total kinematical factor is 2. Note that this does not hold any more if the number of fermion index loop is more than one.

Therefore, remembering that the fermion loops are suppressed by a factor of N_f/N_c, the orbifold equivalence at finite μ_B holds only in the 't Hooft limit (large-N_c limit for fixed N_f) while that at finite μ_I holds both in the 't Hooft and the Veneziano limits (large-N_c limit for fixed N_f/N_c).

One can also argue to what order of $1/N_c$ the orbifold equivalence is valid. The leading corrections to the 't Hooft limit come from the one-fermion-loop planar diagrams, which, as we have shown above, do not distinguish between μ_B and μ_I. Therefore, the difference of the expectation values of gluonic operators, such as the Polyakov loop, between QCD at finite μ_B and μ_I is at most $\sim (N_f/N_c)^2$ due to a two-fermion-loop planar diagram. In particular, the difference of the critical temperature of the deconfinement is $\sim (N_f/N_c)^2$, as previously discussed in [52] without using the orbifold equivalence.

3.3 Condition for the orbifold equivalence and the BEC-BCS crossover region

From the orbifold projections we have constructed, the expectation values of the neutral operators for given T and μ should be identical between the parent and daughter theories. Note here that, in order for the orbifold equivalence to QCD at finite μ_B to hold, the projection symmetry, $\mathbb{Z}_2$ subgroup of the $\mathrm{SO}(2N_c) \times \mathrm{U}(1)_B$ for the $\mathrm{SO}(2N_c)$ gauge theory, or $\mathbb{Z}_2$ subgroup of the $\mathrm{Sp}(2N_c) \times \mathrm{U}(1)_B$ for the $\mathrm{Sp}(2N_c)$ gauge theory, must not be broken spontaneously [32]. However, the $\mathrm{U}(1)_B$ symmetry, whose $\mathbb{Z}_4$ subgroup is used for the projection to QCD at finite μ_B, is broken down to $\mathbb{Z}_2$ inside the BEC-BCS crossover regions in figures 3 and 4. Therefore, the orbifold equivalence to QCD at finite μ_B is valid only outside the BEC-BCS crossover regions. Note that, even at large μ, above the critical temperature of the superfluid, $T > T_c$, the condensates melt away and the equivalence recovers.

On the other hand, the equivalence to QCD at finite μ_I is valid as long as the projection symmetry, $\mathbb{Z}_2$ subgroup of $\mathrm{SO}(2N_c) \times \mathrm{SU}(2)_F$ or $\mathbb{Z}_2$ subgroup of $\mathrm{Sp}(2N_c) \times \mathrm{SU}(2)_F$, is not broken. This condition is satisfied for arbitrary μ and T in all the three theories with flavor symmetry, QCD at finite μ_I and $\mathrm{SO}(2N_c)$ and $\mathrm{Sp}(2N_c)$ gauge theories at finite μ_B. As a result, the chiral condensate $\langle\bar{\psi}\psi\rangle$, the superfluid gap Δ, and their critical temperatures are identical; the phase diagrams characterized by these order parameters completely coincide in the large-N_c limit.

In particular, QCD at finite μ_B is equivalent to QCD at finite μ_I outside the BEC-BCS crossover region. Remembering that dropping the complex phase of the fermion determinant of QCD at finite μ_B reduces to QCD at finite μ_I for $N_f = 2$, this means that *the phase-quenched approximation in this region is exact at large-N_c for neutral operators, e.g., the chiral condensate.* This explains why the phase-quenched approximation works in QCD at high temperature, as already observed in the lattice QCD simulations for small

μ [19] and in model calculations such as the chiral random matrix model [20], Nambu–Jona-Lasinio model [21, 22], and hadron resonance gas model [23]. As we will show in sections 4.2 and 4.3. the results of the chiral random matrix model can also be understood as a consequence of the orbifold equivalence in this model.

3.4 Nonperturbative orbifold equivalence at high density

In Sec. 3.1, we discussed the orbifold equivalence at the perturbative level in the large N_c limit. One might ask if the equivalence does hold nonperturbatively and to what extent the $1/N_c$ corrections are important. For SU(N_c) QCD at large μ_I and SO($2N_c$) and Sp($2N_c$) gauge theories at large μ_B, we can answer both questions for several quantities explicitly. This is because the coupling constants $g_{\rm SU}$, $g_{\rm SO}$, and $g_{\rm Sp}$ are small due to the asymptotic freedom and the calculations are under theoretical control. Note that the weak-coupling does not necessarily mean that calculations are perturbative: as shown in (3.35), (3.36), (3.37), and (3.38) below, the coupling constant dependences of the BCS gaps are indeed nonperturbative. Although our calculations do not constitute the proof of nonperturbative orbifold equivalence for all the neutral observables, they provide a nontrivial piece of evidence for the equivalence.

Let us consider $N_f = 2$. First of all, the chiral condensate $\langle\bar{\psi}\psi\rangle$ is vanishing in all the theories at asymptotically large μ, and the equivalence is trivially satisfied. The nontrivial quantity we can compare is the superfluid gap Δ. Its equivalence is required, e.g., from the equivalence of the fermion occupation number $\langle\psi^\dagger_{af}(t,\mathbf{x})\psi_{bg}(t,\mathbf{y})\rangle$. The gap Δ can be computed using the technique in [53]. The main modification in the gap equations compared with [53] is the group theoretical factor involving N_c given by

$$(T_a^{\rm SU})^T_{\alpha\beta}(T_A^{\rm SU})_{\beta\gamma}(T_a^{\rm SU})_{\gamma\delta} = -\frac{N_c+1}{2N_c}(T_A^{\rm SU})_{\alpha\delta}, \tag{3.31}$$

$$(T_a^{\rm SU})_{\alpha\beta}(\mathbf{1})^{N_c}_{\beta\gamma}(T_a^{\rm SU})_{\gamma\delta} = \frac{N_c^2-1}{2N_c}(\mathbf{1})^{N_c}_{\alpha\delta}, \tag{3.32}$$

$$(T_a^{\rm SO})^T_{\alpha\beta}(\mathbf{1})^{2N_c}_{\beta\gamma}(T_a^{\rm SO})_{\gamma\delta} = -\frac{2N_c-1}{4}(\mathbf{1})^{2N_c}_{\alpha\delta}, \tag{3.33}$$

$$(T_a^{\rm Sp})^T_{\alpha\beta}(J_c)^{2N_c}_{\beta\gamma}(T_a^{\rm Sp})_{\gamma\delta} = -\frac{2N_c+1}{4}(J_c)^{2N_c}_{\alpha\delta}, \tag{3.34}$$

respectively. Solving the gap equations, we obtain the following BCS gap (up to prefactor) for each theory:

$$\Delta^{\rm SU}_{\mu_B} \sim \mu\exp\left(-\frac{\pi^2}{g_{\rm SU}}\sqrt{\frac{6N_c}{N_c+1}}\right), \tag{3.35}$$

$$\Delta^{\rm SU}_{\mu_I} \sim \mu\exp\left(-\frac{\pi^2}{g_{\rm SU}}\sqrt{\frac{6N_c}{N_c^2-1}}\right), \tag{3.36}$$

$$\Delta^{\rm SO}_{\mu_B} \sim \mu\exp\left(-\frac{\pi^2}{g_{\rm SO}}\sqrt{\frac{12}{2N_c-1}}\right), \tag{3.37}$$

$$\Delta^{\rm Sp}_{\mu_B} \sim \mu\exp\left(-\frac{\pi^2}{g_{\rm Sp}}\sqrt{\frac{12}{2N_c+1}}\right). \tag{3.38}$$

Equation (3.35) is the result obtained in [54]. For $N_c = 3$, $\Delta^{\rm SU}_{\mu_B}$ and $\Delta^{\rm SU}_{\mu_I}$ reduce to the results obtained in [53] and [7], respectively. Note that in the 't Hooft limit $\Delta^{\rm SU}_{\mu_I}$, $\Delta^{\rm SO}_{\mu_B}$, and $\Delta^{\rm Sp}_{\mu_B}$ remain finite (and the BEC-BCS crossover regions of these theories do not disappear) while $\Delta^{\rm SU}_{\mu_B}$ is vanishing. This originates from the fact that the diagrams of the one-gluon exchange responsible for $\Delta^{\rm SU}_{\mu_I}$, $\Delta^{\rm SO}_{\mu_B}$, and $\Delta^{\rm Sp}_{\mu_B}$ are planar, whereas it is nonplanar for $\Delta^{\rm SU}_{\mu_B}$ [55, 56]. These consequences are consistent with our claim in Sec. 3.3 that the orbifold equivalence holds between QCD at large μ_I and SO($2N_c$) and Sp($2N_c$) gauge theories at large μ_B while the equivalence with QCD at large μ_B does not hold inside the BEC-BCS crossover region. This gives a simple example in QCD that, if the projection symmetry is broken, the orbifold equivalence is not valid.

Now let us compare $\Delta^{\rm SU}_{\mu_I}$, $\Delta^{\rm SO}_{\mu_B}$, and $\Delta^{\rm Sp}_{\mu_B}$. For the comparisons to the leading order, we take the ratios of the factors in the exponential between (3.36), (3.37), and (3.38). Remembering $g_{\rm SU} = g_{\rm SO} = g_{\rm Sp}$, the ratios read

$$\alpha_{\rm SO/SU}(N_c) = \sqrt{\frac{2(N_c^2-1)}{N_c(2N_c-1)}} = \begin{cases} 1.033 & (N_c = 3) \\ 1 & (N_c = \infty) \end{cases}, \tag{3.39}$$

$$\alpha_{\rm Sp/SU}(N_c) = \sqrt{\frac{2(N_c^2-1)}{N_c(2N_c+1)}} = \begin{cases} 0.873 & (N_c = 3) \\ 1 & (N_c = \infty) \end{cases}. \tag{3.40}$$

Clearly, the equivalence holds in the large-N_c limit between QCD at large μ_I and SO($2N_c$) and Sp($2N_c$) gauge theories at large μ_B. It also turns out that the orbifold equivalence is rather well satisfied even in real QCD, $N_c = 3$. For the complete equivalence of the BCS gap, one has to check if the prefactors in (3.36), (3.37), and (3.38) are also identical, for which subleading effects are important. Here we simply assume the equivalence of the prefactor in the large-N_c limit, and see whether the equivalence of other nonperturbative quantities follow or not.

Provided $\Delta^{\rm SO}_{\mu_I}/\Delta^{\rm SU}_{\mu_B} \to 1$ and $\Delta^{\rm Sp}_{\mu_I}/\Delta^{\rm SU}_{\mu_B} \to 1$ in the large-N_c limit, the critical temperatures T_c of the superfluid phases also coincide with each other, since T_c is proportional to the BCS gap with the universal proportionality factor:

$$T_c = \frac{e^\gamma}{\pi}\Delta, \tag{3.41}$$

where $\gamma \approx 0.577$ is the Euler-Mascheroni constant.

Moreover we compute the magnitudes of the diquark and pion condensates following [54] as

$$\langle \bar{d}\gamma_5 u\rangle^{\rm SU}_{\mu_I} = d^{\rm SU}_{\mu_I}, \qquad |d^{\rm SU}_{\mu_I}| = 2\sqrt{\frac{6N_c}{N_c^2-1}}\frac{\mu^2\Delta^{\rm SU}_{\mu_I}}{\pi g_{\rm SU}}, \tag{3.42}$$

$$\langle \psi^f_a C\gamma_5 \psi^g_b\rangle^{\rm SO}_{\mu_B} = \delta_{ab}\delta^{fg} d^{\rm SO}_{\mu_B}, \qquad |d^{\rm SO}_{\mu_B}| = 2\sqrt{\frac{12}{2N_c-1}}\frac{\mu^2\Delta^{\rm SO}_{\mu_B}}{\pi g_{\rm SO}}, \tag{3.43}$$

$$\langle \psi^f_a C\gamma_5 \psi^g_b\rangle^{\rm Sp}_{\mu_B} = (J_c)_{ab}(J_i)^{fg} d^{\rm Sp}_{\mu_B}, \qquad |d^{\rm Sp}_{\mu_B}| = 2\sqrt{\frac{12}{2N_c+1}}\frac{\mu^2\Delta^{\rm Sp}_{\mu_B}}{\pi g_{\rm Sp}}, \tag{3.44}$$

where J_c and J_i are defined in (2.10) and (3.26). The ratios read

$$\frac{|d^{\rm SO}_{\mu_B}|}{|d^{\rm SU}_{\mu_I}|} = \alpha_{\rm SO/SU}(N_c)\frac{\Delta^{\rm SO}_{\mu_B}}{\Delta^{\rm SU}_{\mu_I}}, \tag{3.45}$$

$$\frac{|d^{\rm Sp}_{\mu_B}|}{|d^{\rm SU}_{\mu_I}|} = \alpha_{\rm Sp/SU}(N_c)\frac{\Delta^{\rm Sp}_{\mu_B}}{\Delta^{\rm SU}_{\mu_I}}, \tag{3.46}$$

where $\alpha_{\rm SO/SU}(N_c)$ and $\alpha_{\rm Sp/SU}(N_c)$ are the quantities defined in (3.39) and (3.40). Both indeed approach unity in the large-N_c limit when $\Delta^{\rm SO}_{\mu_B}/\Delta^{\rm SU}_{\mu_I} \to 1$ and $\Delta^{\rm Sp}_{\mu_B}/\Delta^{\rm SU}_{\mu_I} \to 1$.

Although we did not attempt in this paper, one should also be able to check the equivalence for other quantities at large μ, such as the four-quark condensate $\langle(\bar\psi\psi)(\bar\psi\psi)\rangle$, the pion decay constant f_π, and so on.

3.5 Brief summary

We summarize our results in this section.

1. The whole phase diagrams described by the chiral condensate and the superfluid gap should be universal in the large-N_c limit between QCD at finite μ_I and SO($2N_c$) and Sp($2N_c$) gauge theories at finite μ_B.

2. The phase diagram of QCD at finite μ_B should also be identical to those of other theories above outside the BEC-BCS crossover regions. In particular, the phase-quenched approximation for the chiral condensate is exact in this region.

3. At asymptotically large chemical potentials, the equivalence is rather well satisfied even for $N_c = 3$. From this fact, the phase-quenched approximation for the chiral condensate is expected to work well in real QCD.

4. Orbifold equivalence in the chiral random matrix theories

If the orbifold equivalence holds between the original gauge theories, it is natural to expect that the equivalence should hold at the level of the corresponding low-energy effective theories. In this section, we show that the orbifold equivalence holds perturbatively as well as nonperturbatively in the chiral random matrix theory (RMT), a solvable effective theory of QCD (or QCD-like theory) first introduced in [57]. Actually the RMT has the size of the matrix N, which is taken to infinity (thermodynamic limit) in the end. In this sense, the RMT is a "large-N" matrix model, and hence, the perturbative proof of the orbifold equivalence given in Sec. 3.1 is applicable. Note that the size of the random matrix is not related to the number of color N_c. The orbifold equivalence will be verified nonperturbatively in Sec 4.3 by solving the RMT following [20, 58].

4.1 Chiral random matrix theories

In this subsection, we briefly review the basic aspects of the RMT. For reviews of the RMT in more detail, see [38, 39].

4.1.1 Chiral random matrix theories at small chemical potential

The partition function of the RMT is given by an integral over a Gaussian random matrix ensemble, instead of the average over the gauge field of the original Yang-Mills action:

$$Z = \int d\Phi \prod_{i=1}^{N_f} \det \mathcal{D}\ e^{-\frac{N\beta}{2} G^2 \,\mathrm{tr}\, \Phi^\dagger \Phi}, \tag{4.1}$$

where Φ is an $N \times (N+\nu)$ random matrix element, N is the size of the system, and ν is the topological charge. We also introduced a suitable normalization with the parameter G in the Gaussian. Note that there is no spacetime coordinate in the theory; the size of the matrix N corresponds to the spacetime volume. It is taken to infinity in the end, corresponding to the thermodynamic limit.

The matrix structure of the Dirac operator $\mathcal{D}$ is chosen such that it has the correct anti-unitary symmetries and it reproduces the correct global symmetry breaking pattern of the system. In particular, anti-Hermiticity and chiral symmetry of the Dirac operator at $\mu = m = 0$ require

$$\mathcal{D}^\dagger = -\mathcal{D}, \qquad \{\mathcal{D}, \gamma_5\} = 0. \tag{4.2}$$

The quark mass m, quark chemical potential μ [59], and temperature T [60] can be incorporated into $\mathcal{D}$. While T does not destroy any relation in (4.2), μ and m break the former and the latter relations in (4.2), respectively.

Depending on the anti-unitary symmetries of the Dirac operator, the ensemble is distinguished with the real, complex, or quaternion real [see (4.14) for the definition] matrices denoted by the Dyson index $\beta = 1$, $\beta = 2$, and $\beta = 4$, respectively. The value of β corresponds to the degrees of freedom per matrix element. QCD or QCD-like theory in each universality class and the corresponding RMT is listed as follows [61]:

- The Dirac operator of SU($N_c \geq 3$) QCD has no anti-unitary symmetry and the corresponding RMT belongs to $\beta = 2$. The Dirac operator is taken as

$$\mathcal{D} = \begin{pmatrix} m_f \mathbf{1} & \Phi + \mu \mathbf{1} \\ -\Phi^\dagger + \mu \mathbf{1} & m_f \mathbf{1} \end{pmatrix}, \tag{4.3}$$

  where Φ is an $N \times (N+\nu)$ complex matrix and m_f ($f = 1, 2, \cdots, N_f$) are the quark masses.

- The Dirac operators of SU($N_c = 2$) QCD and Sp($2N_c$) gauge theory have the anti-unitary symmetries, $\mathcal{D} T_2^{\mathrm{SU}} \gamma_5 C = T_2^{\mathrm{SU}} \gamma_5 C \mathcal{D}^*$ and $\mathcal{D} i J_c \gamma_5 C = i J_c \gamma_5 C \mathcal{D}^*$, respectively. Here C is the charge conjugation matrix, T_2^{SU} is the antisymmetric generator of SU(2), and J_c is defined in (2.10). The corresponding RMT belongs to the universality class $\beta = 1$ and the Dirac operator is taken as

$$\mathcal{D} = \begin{pmatrix} m_f \mathbf{1} & \Phi + \mu \mathbf{1} \\ -\Phi^T + \mu \mathbf{1} & m_f \mathbf{1} \end{pmatrix}, \tag{4.4}$$

  where Φ is an $N \times (N+\nu)$ real matrix.

- The Dirac operators of SU(N_c) QCD with adjoint fermions and SO(N_c) gauge theory have the anti-unitary symmetry, $\mathcal{D}\gamma_5 C = \gamma_5 C \mathcal{D}^*$. The corresponding RMT belongs to the universality class $\beta = 4$ and the Dirac operator is taken as

$$\mathcal{D} = \begin{pmatrix} m_f \mathbf{1} & \Phi + \mu \mathbf{1} \\ -\Phi^\dagger + \mu \mathbf{1} & m_f \mathbf{1} \end{pmatrix}, \tag{4.5}$$

  where Φ is a $2N \times 2(N+\nu)$ quaternion real matrix [see (4.14) for the definition].

These RMTs at finite μ can alternatively be formulated by the two-matrix representation [62, 63] where the identity matrix multiplied by μ is replaced by the random matrix element. The effect of temperature T can be incorporated as the (first) Matsubara frequencies by changing $\mu \to \mu + iT$ for one half of the determinant and $\mu \to \mu - iT$ for the other half of the determinant in the simplest model [60].[11]

There is a regime (called the ϵ-regime) where the RMT is exactly equivalent to QCD: when the typical scale of the system L is much smaller than the pion Compton wavelength and is much larger than the inverse of the scale of chiral symmetry breaking [65],

$$\frac{1}{\Lambda_\chi} \ll L \ll \frac{1}{m_\pi}, \qquad \mu L \ll 1, \tag{4.6}$$

QCD reduces to a theory of zero momentum modes of pions. In this regime, the system has a universality, i.e., the dynamics depends only on the symmetry breaking pattern and is independent of the microscopic details; QCD can be replaced by the RMT with the same global symmetry breaking pattern. Outside the ϵ-regime, the universality is lost. However, the RMT is still useful as a schematic model to study the qualitative properties of QCD such as the phase structure at finite T and μ [60]. The advantage of the RMT is that it can be solved analytically although QCD itself cannot be.

4.1.2 Chiral random matrix theories at large chemical potential

Recently, a new class of RMTs which describe the superfluid phase at asymptotically large μ have been identified in [66].[12] The partition function is given by

$$Z = \int dA dB \prod_{i=1}^{N_f} \det \mathcal{D}\ e^{-\frac{N\beta}{2} G^2 \,\mathrm{tr}(A^\dagger A + B^\dagger B)}, \tag{4.7}$$

where A and B are $N \times N$ spacetime independent random matrix elements. Here only the topological sector $\nu = 0$ is considered because the topological susceptibility is strongly suppressed at large μ [69, 70]. Chiral symmetry

$$\{\mathcal{D}, \gamma_5\} = 0, \tag{4.8}$$

[11] Introducing T in this way may break flavor symmetry of the system in some cases. However, the final result is shown to be equivalent to that of the correct prescription preserving flavor symmetry [64].

[12] The mathematical aspects of the same two-matrix model for $\beta = 1$ were previously studied in [67, 68].

is preserved at finite μ in the chiral limit $m = 0$, but anti-Hermiticity of the Dirac operator $\mathcal{D}^\dagger = -\mathcal{D}$ is lost. The non-Hermitian Dirac operator is taken as

$$\mathcal{D} = \begin{pmatrix} m_f \mathbf{1}_N & A_N \\ B_N & m_f \mathbf{1}_N \end{pmatrix}, \tag{4.9}$$

where both A and B are the real, complex, or quaternion real matrices, denoted by the Dyson index $\beta = 1$, $\beta = 2$, and $\beta = 4$, respectively. The $\beta = 1$ RMT corresponds to SU(2) QCD [66] and Sp(N_c) gauge theory at large μ_B, $\beta = 2$ RMT to SU($N_c \geq 3$) QCD at large μ_I, and $\beta = 4$ RMT to adjoint QCD and SO($2N_c$) gauge theory at large μ_B.

We can define the ϵ-regime at large μ where the system has the universality and QCD is equivalent to the RMT [71, 72]:

$$\frac{1}{\Delta} \ll L \ll \frac{1}{m_\pi}, \tag{4.10}$$

where Δ is the BCS gap and m_π is the pion mass associated with chiral symmetry breaking by the diquark condensate (not by the usual chiral condensate). It is shown in [66] that the partition function of the RMT actually coincides with that of the finite-volume effective theory of QCD at large μ.

4.2 Orbifold projections in the chiral random matrix theories

In this section, we construct the orbifold projections in the chiral random matrix theories (RMTs) between $\beta = 4$, $\beta = 2$, and $\beta = 1$. Thereby a class of observables in the RMTs with the different Dyson indices are found to be identical to each other. In the following, we will concentrate on the RMT at finite μ and $T = 0$ introduced in Sec. 4.1.1, which can be easily generalized to nonzero T. For simplicity, we set $\nu = 0$ and consider degenerate quark masses $m_f = m$. The generalizations to the high-density RMTs in Sec. 4.1.2 and to the RMTs in the two-matrix representation [62, 63] are straightforward.

The construction of the orbifold projections is as follows: we start with the $\beta = 4$ or $\beta = 1$ RMT at finite μ_B with the size of the matrix Φ being $2N$, and define the orbifold projection to the $\beta = 2$ RMT at finite μ_B or μ_I with the size of the matrix N. The relations between these RMTs via orbifold projections are summarized in Fig. 6.[13] Each orbifold projection reduces the independent degrees of freedom of the theory to half.

4.2.1 Orbifold projection from $\beta = 4$ to $\beta = 2$

The partition function of the $\beta = 4$ RMT is given by

$$Z = \int d\Phi d\Psi \; e^{-S}, \qquad S = S_B + S_F, \tag{4.11}$$

where

$$S_B = \frac{N\beta}{2} G^2 \,\mathrm{tr}\, \Phi^\dagger \Phi, \qquad S_F = \sum_{f=1}^{N_f} \bar{\Psi}_f \mathcal{D} \Psi_f, \tag{4.12}$$

[13] Although not shown explicitly in this paper, one can also construct the orbifold projection from the $\beta = 2$ RMT at finite μ_I with the size N to the $\beta = 1$ RMT at finite μ_B with the size N.

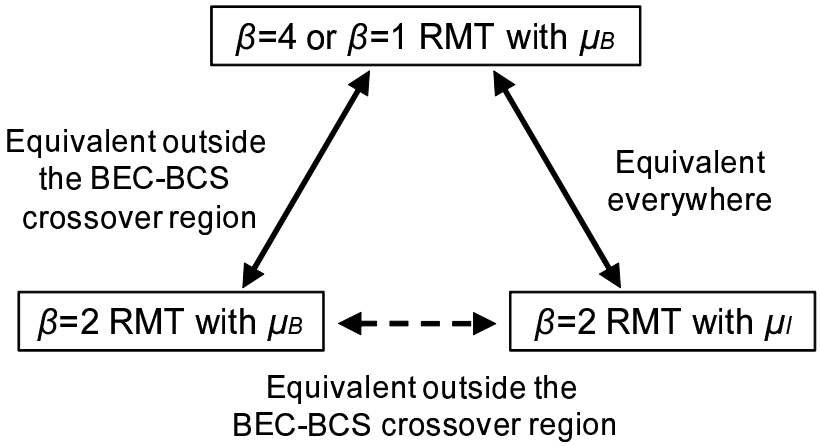

Figure 6: Relations between $\beta = 2$ RMT at finite μ_B or μ_I and $\beta = 4$ and $\beta = 1$ RMTs at finite μ_B. $\beta = 2$ RMT at small and large μ_I can be obtained from $\beta = 4$ and $\beta = 1$ RMTs at small and large μ_B through orbifold projections. $\beta = 2$ RMT at small μ_B can also be obtained from $\beta = 4$ and $\beta = 1$ RMTs at small μ_B while $\beta = 2$ RMT at large μ_B (inside the BEC-BCS crossover region of the parent RMTs) cannot be.

and

$$\mathcal{D} = \begin{pmatrix} m\mathbf{1}_{2N} & \Phi + \mu\mathbf{1}_{2N} \\ -\Phi^\dagger + \mu\mathbf{1}_{2N} & m\mathbf{1}_{2N} \end{pmatrix}. \tag{4.13}$$

Here Ψ_f are complex Grassmann $4N$-component vectors and Φ is a $2N \times 2N$ quaternion real matrix of the form:

$$\Phi \equiv \sum_{\mu=0}^{3} a^\mu i\sigma_\mu = \begin{pmatrix} a^0 + ia^3 & a^2 + ia^1 \\ -a^2 + ia^1 & a^0 - ia^3 \end{pmatrix}, \tag{4.14}$$

where a^μ are $N \times N$ real matrices and $\sigma_\mu = (-i, \sigma_k)$ with Pauli matrices σ_k.

For the bosonic matrix Φ, we impose the projection condition

$$J\Phi J^{-1} = \Phi, \qquad J \equiv \begin{pmatrix} & -\mathbf{1}_N \\ \mathbf{1}_N & \end{pmatrix}. \tag{4.15}$$

Then we obtain

$$\Phi^{\rm proj} = \begin{pmatrix} a^0 & a^2 \\ -a^2 & a^0 \end{pmatrix}, \tag{4.16}$$

which is equivalent to two copies of a $N \times N$ complex matrix after a unitary transformation

$$P\Phi^{\rm proj}P^{-1} = \begin{pmatrix} \phi^* & 0 \\ 0 & \phi \end{pmatrix} \equiv \Phi_{\beta=2}, \qquad P \equiv \frac{1}{\sqrt{2}} \begin{pmatrix} \mathbf{1}_N & i\mathbf{1}_N \\ \mathbf{1}_N & -i\mathbf{1}_N \end{pmatrix}, \tag{4.17}$$

where $\phi = a^0 + ia^2$. The bosonic part of the action is mapped to the one for the $\beta = 2$ RMT. Note that the factor 2 in the recipe (3.15) is reflected in the difference of normalization

between $\beta = 4$ and $\beta = 2$ in (4.12) if the trace for $\beta = 4$ is understood as the so-called "QTr" which is one-half the usual trace.

In order to introduce a projection for the fermions, we write Ψ by using two $2N$-component fermions ψ_R and ψ_L as

$$\Psi = \begin{pmatrix} \psi_R \\ \psi_L \end{pmatrix}. \tag{4.18}$$

Here ψ_R and ψ_L are further decomposed into two N-component fermions

$$\psi_R = \begin{pmatrix} \psi_R^1 \\ \psi_R^2 \end{pmatrix}, \qquad \psi_L = \begin{pmatrix} \psi_L^1 \\ \psi_L^2 \end{pmatrix}, \tag{4.19}$$

where the flavor index is suppressed for simplicity. The projection to the $\beta = 2$ RMT at finite μ_B is given by

$$\psi_R = \omega J \psi_R, \qquad \psi_L = \omega J \psi_L, \tag{4.20}$$

where $\omega = e^{i\pi/2}$ as defined in Sec. 3.2. Performing the unitary transformation, we have

$$P\psi_R^{\rm proj} = \begin{pmatrix} 0 \\ \psi_R^- \end{pmatrix}, \qquad P\psi_L^{\rm proj} = \begin{pmatrix} 0 \\ \psi_L^- \end{pmatrix}, \tag{4.21}$$

where $\psi_R^\pm = (\psi_R^1 \pm i\psi_R^2)/\sqrt{2}$ and $\psi_L^\pm = (\psi_L^1 \pm i\psi_L^2)/\sqrt{2}$. The fermionic part of the action reads

$$(0, \bar\psi_L^-, 0, \bar\psi_R^-) \begin{pmatrix} m\mathbf{1}_N & 0 & \phi^* + \mu\mathbf{1}_N & 0 \\ 0 & m\mathbf{1}_N & 0 & \phi + \mu\mathbf{1}_N \\ -\phi^T + \mu\mathbf{1}_N & 0 & m\mathbf{1}_N & 0 \\ 0 & -\phi^\dagger + \mu\mathbf{1}_N & 0 & m\mathbf{1}_N \end{pmatrix} \begin{pmatrix} 0 \\ \psi_R^- \\ 0 \\ \psi_L^- \end{pmatrix} = 2\bar\Psi_{\beta=2}\mathcal{D}(\mu)_{\beta=2}\Psi_{\beta=2}, \tag{4.22}$$

where

$$\mathcal{D}(\mu)_{\beta=2} = \begin{pmatrix} m\mathbf{1}_N & \phi + \mu\mathbf{1}_N \\ -\phi^\dagger + \mu\mathbf{1}_N & m\mathbf{1}_N \end{pmatrix}, \qquad \Psi_{\beta=2} = \frac{1}{\sqrt{2}} \begin{pmatrix} \psi_R^- \\ \psi_L^- \end{pmatrix}. \tag{4.23}$$

This is the $\beta = 2$ RMT at finite quark chemical potential μ.

In order to obtain the $\beta = 2$ RMT at finite μ_I, we impose the projection condition:

$$J\psi_R J_i^{-1} = \psi_R, \qquad J\psi_L J_i^{-1} = \psi_L. \tag{4.24}$$

If we define $\varphi_R^\pm = (\psi_{Rf}^\pm \mp i\psi_{Rg}^\pm)/\sqrt{2}$ and $\xi_R^\pm = (\psi_{Rf}^\pm \pm i\psi_{Rg}^\pm)/\sqrt{2}$ (and similarly for $\varphi_L^\pm$ and $\xi_L^\pm$) with f and g being the flavor indices, the fermions $\varphi_{R,L}^\pm$ survive but $\xi_{R,L}^\pm$ disappear after the projection. The fermionic part of the action reads

$$\begin{aligned} &(\bar\varphi_L^+, \bar\varphi_L^-, \bar\varphi_R^+, \bar\varphi_R^-) \begin{pmatrix} m\mathbf{1}_N & 0 & \phi^* + \mu\mathbf{1}_N & 0 \\ 0 & m\mathbf{1}_N & 0 & \phi + \mu\mathbf{1}_N \\ -\phi^T + \mu\mathbf{1}_N & 0 & m\mathbf{1}_N & 0 \\ 0 & -\phi^\dagger + \mu\mathbf{1}_N & 0 & m\mathbf{1}_N \end{pmatrix} \begin{pmatrix} \varphi_R^+ \\ \varphi_R^- \\ \varphi_L^+ \\ \varphi_L^- \end{pmatrix} \\ &= 2\left[\bar\Psi_{\beta=2}^+ \mathcal{D}(-\mu)_{\beta=2}\Psi_{\beta=2}^+ + \bar\Psi_{\beta=2}^- \mathcal{D}(\mu)_{\beta=2}\Psi_{\beta=2}^-\right], \end{aligned} \tag{4.25}$$

where

$$\Psi^+_{\beta=2} = \frac{1}{\sqrt{2}} \begin{pmatrix} (\varphi^+_R)^C \\ (\varphi^+_L)^C \end{pmatrix}, \qquad \Psi^-_{\beta=2} = \frac{1}{\sqrt{2}} \begin{pmatrix} \varphi^-_R \\ \varphi^-_L \end{pmatrix}. \tag{4.26}$$

Because Ψ^- and Ψ^+ have the quark chemical potential $+\mu$ and $-\mu$ respectively, it is the $\beta = 2$ RMT at finite isospin chemical potential $\mu_I = 2\mu$.

4.2.2 Orbifold projection from $\beta = 1$ to $\beta = 2$

The $\beta = 2$ RMT can also be obtained from the $\beta = 1$ RMT. We start with the action of the $\beta = 1$ RMT given by (4.12), but the Dirac operator is now

$$\mathcal{D} = \begin{pmatrix} m\mathbf{1}_{2N} & \Phi + \mu\mathbf{1}_{2N} \\ -\Phi^T + \mu\mathbf{1}_{2N} & m\mathbf{1}_{2N} \end{pmatrix}, \tag{4.27}$$

where Φ is a $2N \times 2N$ real matrix. Φ can be parametrized as

$$\Phi = \begin{pmatrix} a^0 + a^3 & a^2 + a^1 \\ -a^2 + a^1 & a^0 - a^3 \end{pmatrix}, \tag{4.28}$$

where a^μ are $N \times N$ real matrices. Note that the only change in this expression compared with (4.14) is that the factors i in front of a^0 and a^3 are absent. Then one can easily find that the same projection conditions for Φ and Ψ as Sec. 4.2.1 give the $\beta = 2$ RMT at finite μ or finite μ_I.

4.3 Solving the chiral random matrix theories

The orbifold equivalence in the RMT predicts that the $\beta = 4$ and $\beta = 1$ RMTs at finite μ_B and $\beta = 2$ RMT at finite μ_I are equivalent to each other in the neutral sector. Moreover, outside the superfluid phase, the above three theories must also be equivalent to the $\beta = 2$ RMT at finite μ_B. In this section, we will verify these statements at the nonperturbative level by computing the effective potential of each RMT.

For the $\beta = 2$ and $\beta = 1$ RMTs, the effective potentials are computed in [20, 58]. The equivalence of the effective potential of the $\beta = 2$ RMT at finite μ_B (at $\mu_I = 0$) and that of the $\beta = 2$ RMT at finite μ_I (at $\mu_B = 0$) is pointed out outside the pion condensed phase. Here we show that the equivalence holds between a larger class of RMTs as a natural consequence of the orbifold projections constructed in the previous subsection.

Let us sketch the derivation of the effective potential of the RMT. First, introduce the Grassmann vectors (fermions) ψ to write the determinant into an exponential form. Second, perform the Gaussian integration over the matrix element Φ, which leads to the four-fermion term in the exponent. Third, introduce the bosonic auxiliary field A to make it the fermion bilinears (this procedure is called the Hubbard-Stratonovich transformation). Fourth, perform the Gaussian integration over Ψ. Finally, the effective potential is given as the saddle point of the integrand in the $N \to \infty$ limit (the thermodynamic limit).[14]

[14] Our arguments depend on the ansatz of the saddle point of A (defined below) at finite T and μ similarly to [20, 58].

In the following, we consider the $N_f = 2$ RMT in (4.1) with the quark mass m_f and the chemical potential μ_f for each flavor, $f = 1, 2$. The baryon and isospin chemical potentials are defined as

$$\bar{\mu}_B \equiv \frac{\mu_B}{N_c} = \frac{1}{2}(\mu_1 + \mu_2), \tag{4.29}$$

$$\bar{\mu}_I \equiv \frac{\mu_I}{2} = \frac{1}{2}(\mu_1 - \mu_2). \tag{4.30}$$

We denote the chiral condensate as σ_f, pion condensate as ρ, diquark condensate as Δ, and their sources as m_f, λ, and J, respectively.

4.3.1 Effective potential of $\beta = 4$

We first consider the $\beta = 4$ RMT with degenerate quark mass $m_f = m$ at finite baryon chemical potential $\mu_f = \bar{\mu}_B$ (and hence $\sigma_f = \sigma$). We will focus on $T = 0$ and introduce T later changing as $\bar{\mu}_B \to \bar{\mu}_B + iT$ and $\bar{\mu}_B \to \bar{\mu}_B - iT$ for each half of the fermion determinant following [64].

Remembering the definition of the quaternion real matrix (4.14), the partition function can be rewritten as

$$\begin{aligned} Z = \int da^\mu d\psi^* d\psi \ \exp\Big[& -2NG^2 \operatorname{tr}(a_\mu a_\mu^T) + \psi^{f*}_{Ri}(a^\mu_{ij} i\sigma_\mu + \bar{\mu}_B \mathbf{1}_{ij})\psi^f_{Lj} \\ & -\psi^g_{Ri}(a^\mu_{ij} i\sigma^*_\mu + \bar{\mu}_B \mathbf{1}_{ij})\psi^{g*}_{Lj} + M^\dagger_{fg}\psi^{f*}_{Ri}\psi^g_{Ri} + M_{fg}\psi^{f*}_{Lj}\psi^g_{Lj}\Big], \end{aligned} \tag{4.31}$$

where $\psi_{R,L}$ are the Grassmann $2N$-component vectors and f, g are flavor indices and i, j run over $1, 2, \cdots 2N$. Integrating out a_μ and using the Fierz identity,

$$(\sigma_\mu)^{ab}(\sigma^*_\mu)^{cd} = 2\delta_{ac}\delta_{db}, \tag{4.32}$$

the partition function reduces to

$$\begin{aligned} Z = \int d\psi^* d\psi \ \exp\Bigg[& \frac{1}{2NG^2}(\psi^{f*}_{Ri}\psi^g_{Ri})(\psi^{g*}_{Lj}\psi^f_{Lj}) + \bar{\mu}_B(\psi^{f*}_{Ri}\psi^f_{Li} + \psi^{g*}_{Lj}\psi^g_{Rj}) \\ & + M^\dagger_{fg}\psi^{f*}_{Ri}\psi^g_{Ri} + M_{fg}\psi^{f*}_{Lj}\psi^g_{Lj}\Bigg]. \end{aligned} \tag{4.33}$$

Performing the Hubbard-Stratonovich transformation by introducing the auxiliary real and symmetric $N_f \times N_f$ matrices K_{fg} and L_{fg}, one has

$$\begin{aligned} Z = \int dK dL d\psi^* d\psi \exp\big[& -8NG^2 \operatorname{tr}(K^2 + L^2) + \bar{\mu}_B(\psi^{f*}_{Ri}\psi^f_{Li} + \psi^{g*}_{Lj}\psi^g_{Rj}) \\ & + 2\psi^{f*}_{Ri}\psi^g_{Ri}(K + iL)_{fg} + 2\psi^{g*}_{Lj}\psi^f_{Lj}(K - iL)_{fg} \\ & + M^\dagger_{fg}\psi^{f*}_{Ri}\psi^g_{Ri} + M_{fg}\psi^{f*}_{Lj}\psi^g_{Lj}\Big]. \end{aligned} \tag{4.34}$$

Integrating over the fermionic variables ψ and ψ^* leads to the expression:

$$Z = \int dA \exp[-N\Omega_{\beta=4}(A, A^\dagger)], \tag{4.35}$$

where $\Omega_{\beta=4}$ is an effective potential given by

$$\Omega_{\beta=4} = 8G^2\,\mathrm{tr}(AA^\dagger) - 2\log\det Q. \tag{4.36}$$

Here $A = K - iL$ is the complex and symmetric $N_f \times N_f$ matrix and

$$Q = \begin{pmatrix} 2A^\dagger + M^\dagger & \bar{\mu}_B\delta_{fg} \\ \bar{\mu}_B\delta_{fg} & 2A + M \end{pmatrix}. \tag{4.37}$$

We set the source term M and make the ansatz for A as follows,

$$M = \begin{pmatrix} m & iJ \\ iJ & m \end{pmatrix}, \qquad A = \begin{pmatrix} \sigma & i\Delta \\ i\Delta & \sigma \end{pmatrix}. \tag{4.38}$$

Shifting σ and Δ such that m and J dependences are absorbed into the quadratic term and adding the T-dependence, one finally arrives at the effective potential of $\beta = 4$ RMT:

$$\Omega_{\beta=4} = 16G^2\left[\left(\sigma - \frac{m}{2}\right)^2 + \left(\Delta - \frac{J}{2}\right)^2\right] - 2\sum_{\pm}\ln[4\sigma^2 + 4\Delta^2 - (\bar{\mu}_B \pm iT)^2]. \tag{4.39}$$

The chiral condensate and the diquark condensate are expressed using σ and Δ as

$$\langle\bar{u}u\rangle_{\beta=4} = \frac{1}{4N}\partial_m \ln Z_{\beta=4}\Big|_{m=0} = -4G^2\sigma_{\beta=4}, \tag{4.40}$$

$$\langle u^T C\gamma_5 u\rangle_{\beta=4} = \frac{1}{4N}\partial_J \ln Z_{\beta=4}\Big|_{J=0} = -4G^2\Delta_{\beta=4}. \tag{4.41}$$

4.3.2 Effective potential of $\beta = 2$

Similarly to the case with $\beta = 4$, one can obtain the effective potential of $\beta = 2$ RMT. This was previously computed in [20] and the result reads

$$\begin{aligned}\Omega_{\beta=2} = {} & G^2[(\sigma_1 - m_1)^2 + (\sigma_2 - m_2)^2 + 2(\rho - \lambda)^2] \\ & -\frac{1}{2}\sum_{\pm}\ln[(\sigma_1 + \mu_1 \pm iT)(\sigma_2 - \mu_2 \mp iT) + \rho^2][(\sigma_1 - \mu_1 \mp iT)(\sigma_2 + \mu_2 \pm iT) + \rho^2].\end{aligned} \tag{4.42}$$

The chiral condensate and pion condensate are calculated as

$$\langle\bar{u}u\rangle_{\beta=2} = \frac{1}{2N}\partial_{m_1} \ln Z_{\beta=2}\Big|_{m_1=0} = -G^2\sigma_{\beta=2}, \tag{4.43}$$

$$\langle\bar{d}\gamma^5 u\rangle_{\beta=2} = \frac{1}{4N}\partial_\lambda \ln Z_{\beta=2}\Big|_{\lambda=0} = -G^2\rho_{\beta=2}. \tag{4.44}$$

Note that, as long as $\rho = 0$ (i.e., outside the pion condensed phase), the potential (4.42) is a function of $\mu_1^2 = (\bar{\mu}_B + \bar{\mu}_I)^2$ and $\mu_2^2 = (\bar{\mu}_B - \bar{\mu}_I)^2$. This property leads to the relation:

$$\Omega_{\beta=2}(\bar{\mu}_B)|_{\bar{\mu}_I=0} = \Omega_{\beta=2}(\bar{\mu}_I)|_{\bar{\mu}_B=0} \quad \text{for} \quad \rho = 0. \tag{4.45}$$

Here $\rho = 0$ is the condition that the projection symmetry, which is used for the orbifolding in Sec. 4.2, is not broken spontaneously. From (4.45), the magnitude of the chiral condensate σ and the critical temperature of chiral phase transition T^σ in each theory coincide,

$$\sigma_{\beta=2}(\bar{\mu}_B)|_{\bar{\mu}_I=0} = \sigma_{\beta=2}(\bar{\mu}_I)|_{\bar{\mu}_B=0} \quad \text{for} \quad \rho = 0, \tag{4.46}$$

$$T^\sigma_{\beta=2}(\bar{\mu}_B)|_{\bar{\mu}_I=0} = T^\sigma_{\beta=2}(\bar{\mu}_I)|_{\bar{\mu}_B=0} \quad \text{for} \quad \rho = 0, \tag{4.47}$$

as a consequence of the orbifold equivalence. Especially, this shows that the phase-quenched approximation for $\sigma_{\beta=2}(\bar{\mu}_B)$ and $T^\sigma_{\beta=2}(\bar{\mu}_B)$ works outside the pion condensed phase, as mentioned in [20].

It should be remarked that, even though the effective potentials are identical in (4.45) for $\rho = 0$, the partition functions themselves are not generally the same. This is because the preexponential factor also contributes to the partition function, which is not taken into account in computing the effective potential.[15] Therefore, the sign problem measured as the phase of the partition function can be severe inside as well as outside the pion condensed phase [73]. The result here shows that the phase-quenched approximation is exact for the observables above independently of the severity of the sign problem, as long as $\rho = 0$.

4.3.3 Effective potential of $\beta = 1$

The effective potential of $\beta = 1$ RMT is computed in [58] as

$$\begin{aligned}
\Omega_{\beta=1} = {} & G^2[(\sigma_1 - m_1)^2 + (\sigma_2 - m_2)^2 + 2(\rho - \lambda)^2 + 2(\Delta - J)^2] \\
& -\frac{1}{4}\sum_{\pm} \ln\{[(\sigma_1 + \mu_1 \pm iT)(\sigma_2 - \mu_2 \mp iT) + \rho^2 + \Delta^2] \\
& \qquad \times[(\sigma_1 - \mu_1 \pm iT)(\sigma_2 + \mu_2 \mp iT) + \rho^2 + \Delta^2] + 4\Delta^2\mu_1\mu_2\} \\
& \qquad \times\{[(\sigma_1 - \mu_1 \mp iT)(\sigma_2 + \mu_2 \pm iT) + \rho^2 + \Delta^2] \\
& \qquad \times(\sigma_1 + \mu_1 \mp iT)(\sigma_2 - \mu_2 \pm iT) + \rho^2 + \Delta^2] + 4\Delta^2\mu_1\mu_2\}.
\end{aligned} \tag{4.48}$$

The chiral condensate, pion condensate, and diquark condensate read

$$\langle \bar{u}u \rangle_{\beta=1} = \frac{1}{2N}\partial_{m_1} \ln Z_{\beta=1}\Big|_{m_1=0} = -G^2\sigma_{\beta=1}, \tag{4.49}$$

$$\langle \bar{d}\gamma^5 u \rangle_{\beta=1} = \frac{1}{4N}\partial_{\lambda} \ln Z_{\beta=1}\Big|_{\lambda=0} = -G^2\rho_{\beta=1}. \tag{4.50}$$

$$\langle d^T C\gamma_5 u \rangle_{\beta=1} = \frac{1}{4N}\partial_{J} \ln Z_{\beta=1}\Big|_{J=0} = -G^2\Delta_{\beta=1}. \tag{4.51}$$

The potential (4.48) has the symmetry

$$\Omega_{\beta=1}(\Delta, \rho, \mu_1, \mu_2) = \Omega_{\beta=1}(\rho, -\Delta, \mu_1, -\mu_2), \tag{4.52}$$

due to the $\bar{\mu}_B \leftrightarrow \bar{\mu}_I$ symmetry for $\beta = 1$. Note that this symmetry has nothing to do with the orbifold equivalence.

[15] For $\rho \neq 0$, the partition functions are not identical even in the leading exponential behavior.

4.3.4 Nonperturbative orbifold equivalence between $\beta = 4$, $\beta = 2$, and $\beta = 1$

Comparing (4.39), (4.42), and (4.48), and using the $\bar{\mu}_B \leftrightarrow \bar{\mu}_I$ symmetry for $\beta = 1$ RMT, one finds the relation (note that $\Delta = 0$ at $\bar{\mu}_B = 0$ and $\rho = 0$ at $\bar{\mu}_I = 0$):

$$\Omega_{\beta=4}(\bar{\mu}_B)|_{\bar{\mu}_I=0} = 2\Omega_{\beta=2}(\bar{\mu}_I)|_{\bar{\mu}_B=0} = 2\Omega_{\beta=1}(\bar{\mu}_B)|_{\bar{\mu}_I=0}, \tag{4.53}$$

$$\text{for} \quad 2\sigma_{\beta=4} = \sigma_{\beta=2} = \sigma_{\beta=1}, \quad 2\Delta_{\beta=4} = \rho_{\beta=2} = \Delta_{\beta=1}. \tag{4.54}$$

Unlike the relation (4.45), this is valid not only for $\rho = 0$ (or $\Delta = 0$) but also for $\rho \neq 0$ (or $\Delta \neq 0$), as is consistent with our claim in Sec. 3.3. The difference of the factor 2 in (4.53) originates from the recipe (3.15), or the fact that the $\beta = 4$ RMT with the size of the matrix Φ being $2N$ includes 2 copies of the $\beta = 2$ or $\beta = 1$ RMT with the size N. The factors 2 in (4.54) originate from the identifications of the chiral condensate and diquark (or pion) condensate according to the recipe (3.15) again, e.g., $\langle \bar{u}u \rangle_{\beta=4} = 2\langle \bar{u}u \rangle_{\beta=2} = 2\langle \bar{u}u \rangle_{\beta=1}$. The relation (4.53) leads to the equivalence of the magnitudes of the order parameters (up to the factor 2) and the critical temperatures:

$$2\sigma_{\beta=4}(\bar{\mu}_B)|_{\bar{\mu}_I=0} = \sigma_{\beta=2}(\bar{\mu}_I)|_{\bar{\mu}_B=0} = \sigma_{\beta=1}(\bar{\mu}_B)|_{\bar{\mu}_I=0}, \tag{4.55}$$

$$2\Delta_{\beta=4}(\bar{\mu}_B)|_{\bar{\mu}_I=0} = \rho_{\beta=2}(\bar{\mu}_I)|_{\bar{\mu}_B=0} = \Delta_{\beta=1}(\bar{\mu}_B)|_{\bar{\mu}_I=0}, \tag{4.56}$$

$$T^{\sigma}_{\beta=4}(\bar{\mu}_B)|_{\bar{\mu}_I=0} = T^{\sigma}_{\beta=2}(\bar{\mu}_I)|_{\bar{\mu}_B=0} = T^{\sigma}_{\beta=1}(\bar{\mu}_B)|_{\bar{\mu}_I=0}, \tag{4.57}$$

$$T^{\Delta}_{\beta=4}(\bar{\mu}_B)|_{\bar{\mu}_I=0} = T^{\rho}_{\beta=2}(\bar{\mu}_I)|_{\bar{\mu}_B=0} = T^{\Delta}_{\beta=1}(\bar{\mu}_B)|_{\bar{\mu}_I=0}, \tag{4.58}$$

as a consequence of the orbifold equivalence. We note that, the equivalence of the neutral order parameters and the critical temperatures should be satisfied in the original QCD and QCD-like theories as we claimed in Sec. 3, while the effective potentials will not necessarily coincide in QCD as (4.53). In the case of the RMT, the effective potential is a function of only the neutral order parameters and all the moments are identical; as a result, the effective potentials must be identical. In QCD and QCD-like theories, the effective potentials are functions of not only the neutral order parameters but also non-neutral ones, so the effective potentials will not be identical generally.

4.4 Brief summary

We have applied the idea of the orbifold equivalence to the chiral random matrix theories (RMTs) and constructed the orbifold projections between the RMTs with different Dyson indices β. The equivalence of the order parameters, both the chiral condensate and diquark (or pion) condensate, has been demonstrated by computing the effective potentials of RMTs.

From the viewpoint of the orbifold projection, the construction of whole class of the RMTs at finite μ can be understood in a unified way (see Fig. 6). However, the $\beta = 2$ RMT at large μ_B is the only exception among these RMTs which cannot be obtained through the orbifold projection from the parent RMT because of the spontaneous breaking of the projection symmetry. This may be the fundamental reason why an RMT at large μ_B which reproduces the partition function of the color-flavor locked phase in the ϵ-regime [71] has not been constructed yet.

5. Conclusion and discussions

In this paper, we have discussed the universality of the phase diagrams of QCD and QCD-like theories in the large-N_c limit via the orbifold equivalence. The whole phase diagrams described by the chiral condensate and the superfluid gap are identical between SU(N_c) QCD at finite isospin chemical potential μ_I and SO($2N_c$) and Sp($2N_c$) gauge theories at finite baryon chemical potential μ_B. The phase diagrams of these theories outside the BEC-BCS crossover regions are also identical to that of SU(N_c) QCD at finite μ_B. Especially, the chiral condensate and its critical temperature in QCD at finite μ_B should be exactly described by those of sign-free QCD at finite μ_I: the phase-quenched approximation for these quantities is exact in the large-N_c limit outside the BEC-BCS crossover region.[16] We have also checked that the equivalence is well satisfied for $N_c = 3$ at asymptotically high densities using the controlled weak-coupling calculations. This leads us to expect that the phase-quenched approximation for the chiral condensate also works well even for $N_c = 3$.

Our results provide a way to evade the sign problem in the lattice QCD simulation at finite μ_B, especially in the region relevant to the physics of the chiral phase transition at high temperature. The putative QCD critical point may be investigated by studying the sign-free QCD at finite μ_I and SO($2N_c$) and Sp($2N_c$) gauge theories at finite μ_B outside the BEC-BCS crossover regions. The lattice QCD simulations in QCD at finite μ_I were already performed in [74, 75] which seem consistent with the results at finite μ_B [76, 77] though they may not be conclusive. Further investigations in this direction would be desirable.

Other interesting phenomena in QCD at large μ_B and at low T, such as the color superconductivity [3] and the quarkyonic phase [78, 79], are unfortunately inside the BEC-BCS crossover region of the parent SO and Sp gauge theories where the orbifold equivalence breaks down. One may add appropriate deformation to SO($2N_c$) [35, 36] and Sp($2N_c$) gauge theories to prevent the BEC of diquark pairing at small μ, which allows us to study the properties of QCD beyond $\mu = m_\pi/2$ using the lattice technique. One should note, however, that it is this BEC-BCS crossover region inside which the QCD phase diagram at finite μ_B crucially depends on N_c. For example, the color superconductivity is no longer energetically favorable and is replaced by the inhomogeneous chiral density wave in the 't Hooft limit [55, 56]. This is in contrast to QCD at finite μ_B outside the BEC-BCS crossover region, QCD at finite μ_I, and SO($2N_c$) and Sp($2N_c$) gauge theories at finite μ_B, where the phase structures are not affected by N_c qualitatively. There might be some

[16] One might suspect that, for $\mu < m_\pi/2$ and small but finite T, the system is a gas of baryons in QCD at finite μ_B, which is completely different from a gas of pions in QCD at finite μ_I, and the equivalence would not hold. However, this difference is irrelevant to the orbifold equivalence of the neutral operators in the large-N_c limit. For example, consider the chiral condensate at small T. In QCD at finite μ_B, the thermal excitation of heavy baryons with the mass $\sim N_c^1$ is suppressed at small $T = \mathcal{O}(N_c^0)$ so that the chiral condensate remains unchanged from the value in the QCD vacuum. On the other hand, in QCD at finite μ_I, the thermal excitation of pions with the mass $\sim N_c^0$ cannot change the chiral condensate $\sim N_c^1$. Therefore, the magnitude of the chiral condensate should be the same in both theories in this region, and the equivalence is satisfied rather trivially. The prediction of the orbifold equivalence is nontrivial at larger T near the critical temperature $T_c(\mu)$ of the chiral phase transition; if it is larger than the critical temperature of the deconfinement phase transition, it generally depends on μ, for which the orbifold equivalence still predicts the exactly the same $T_c(\mu)$ in both theories.

connection between the region where the physics dramatically changes depending on N_c and the region where the orbifold equivalence breaks down.

As we have revealed in this paper, the idea of the orbifold equivalence is useful to discuss the universal properties of different quantum field theories. One should be able to see the universality of phase diagrams in QCD and QCD-like theories within a holographic model of QCD, the Sakai-Sugimoto model [80] and its generalizations to SO($2N_c$) and Sp($2N_c$) gauge groups [81]. It would also be interesting to argue possible universal properties of other systems than QCD. For example, one may generalize the orbifold equivalence in the chiral random matrix theories to other class of random matrix theories (Wigner-Dyson type and Bogoliubov-de Gennes type) relevant to other systems.

Note added

Further study [82] reveals that the QCD critical point is theoretically ruled out in QCD at finite μ_B outside the BEC-BCS crossover regions in the corresponding phase diagrams of QCD at finite μ_I and SO($2N_c$) and Sp($2N_c$) gauge theories at finite μ_B, at least in the large-N_c limit.

Acknowledgement

The authors would like to thank A. Cherman, C. Hoyos-Badajoz, A. Karch, B. Tiburzi, and L. Yaffe for stimulating discussions and comments. The works of M. H. and N. Y. are supported by Japan Society for the Promotion of Science Postdoctoral Fellowships for Research Abroad.

References

[1] K. Fukushima and T. Hatsuda, "The phase diagram of dense QCD," Rept. Prog. Phys. **74**, 014001 (2011) [arXiv:1005.4814 [hep-ph]].

[2] M. A. Stephanov, "QCD phase diagram and the critical point," Prog. Theor. Phys. Suppl. **153**, 139 (2004) [arXiv:hep-ph/0402115].

[3] M. G. Alford, A. Schmitt, K. Rajagopal and T. Schäfer, "Color superconductivity in dense quark matter," Rev. Mod. Phys. **80**, 1455 (2008) [arXiv:0709.4635 [hep-ph]].

[4] J. B. Kogut, M. A. Stephanov and D. Toublan, "On two-color QCD with baryon chemical potential," Phys. Lett. B **464**, 183 (1999) [arXiv:hep-ph/9906346].

[5] J. B. Kogut, M. A. Stephanov, D. Toublan, J. J. M. Verbaarschot and A. Zhitnitsky, "QCD-like theories at finite baryon density," Nucl. Phys. B **582**, 477 (2000) [arXiv:hep-ph/0001171].

[6] M. G. Alford, A. Kapustin and F. Wilczek, "Imaginary chemical potential and finite fermion density on the lattice," Phys. Rev. D **59**, 054502 (1999) [arXiv:hep-lat/9807039].

[7] D. T. Son and M. A. Stephanov, "QCD at finite isospin density," Phys. Rev. Lett. **86**, 592 (2001) [arXiv:hep-ph/0005225].

[8] C. Lovelace, "Universality At Large N," Nucl. Phys. **B201**, 333 (1982).

[9] M. Unsal, "Phases of $N_c = \infty$ QCD-like gauge theories on $S^3 \times S^1$ and nonperturbative orbifold-orientifold equivalences," Phys. Rev. D **76**, 025015 (2007) [arXiv:hep-th/0703025].

[10] D. M. Eagles, "Possible Pairing without Superconductivity at Low Carrier Concentrations in Bulk and Thin-Film Superconducting Semiconductors," Phys. Rev. **186**, 456 (1969).

[11] A. J. Leggett, "Cooper pairing in spin-polarized Fermi systems," J. Phys. **41**, C7-19 (1980).

[12] P. Nozières and S. Schmitt-Rink, "Bose condensation in an attractive fermion gas: From weak to strong coupling superconductivity," J. Low. Temp. Phys. **59** 195 (1985).

[13] T. Schäfer and F. Wilczek, "Continuity of quark and hadron matter," Phys. Rev. Lett. **82**, 3956 (1999) [arXiv:hep-ph/9811473].

[14] T. Hatsuda, M. Tachibana, N. Yamamoto and G. Baym, "New critical point induced by the axial anomaly in dense QCD," Phys. Rev. Lett. **97**, 122001 (2006) [arXiv:hep-ph/0605018].

[15] N. Yamamoto, M. Tachibana, T. Hatsuda and G. Baym, "Phase structure, collective modes, and the axial anomaly in dense QCD," Phys. Rev. **D76**, 074001 (2007) [arXiv:0704.2654 [hep-ph]].

[16] M. Kitazawa, D. H. Rischke and I. A. Shovkovy, "Bound diquarks and their Bose-Einstein condensation in strongly coupled quark matter," Phys. Lett. B **663**, 228 (2008) [arXiv:0709.2235 [hep-ph]].

[17] H. Abuki, G. Baym, T. Hatsuda and N. Yamamoto, "The NJL model of dense three-flavor matter with axial anomaly: the low temperature critical point and BEC-BCS diquark crossover," Phys. Rev. D **81**, 125010 (2010) [arXiv:1003.0408 [hep-ph]].

[18] K. Splittorff, D. T. Son and M. A. Stephanov, "QCD - like theories at finite baryon and isospin density," Phys. Rev. D **64**, 016003 (2001) [arXiv:hep-ph/0012274].

[19] C. R. Allton *et al.*, "The QCD thermal phase transition in the presence of a small chemical potential," Phys. Rev. D **66**, 074507 (2002) [arXiv:hep-lat/0204010].

[20] B. Klein, D. Toublan and J. J. M. Verbaarschot, "The QCD phase diagram at nonzero temperature, baryon and isospin chemical potentials in random matrix theory," Phys. Rev. D **68**, 014009 (2003) [arXiv:hep-ph/0301143].

[21] D. Toublan and J. B. Kogut, "Isospin chemical potential and the QCD phase diagram at nonzero temperature and baryon chemical potential," Phys. Lett. B **564**, 212 (2003) [arXiv:hep-ph/0301183].

[22] A. Barducci, R. Casalbuoni, G. Pettini and L. Ravagli, "A NJL-based study of the QCD critical line," Phys. Rev. D **72**, 056002 (2005) [arXiv:hep-ph/0508117].

[23] D. Toublan and J. B. Kogut, "The QCD phase diagram at nonzero baryon, isospin and strangeness chemical potentials: Results from a hadron resonance gas model," Phys. Lett. B **605**, 129 (2005) [arXiv:hep-ph/0409310].

[24] S. Kachru and E. Silverstein, "4d conformal theories and strings on orbifolds," Phys. Rev. Lett. **80**, 4855 (1998) [arXiv:hep-th/9802183].

[25] A. E. Lawrence, N. Nekrasov and C. Vafa, "On conformal field theories in four-dimensions," Nucl. Phys. **B533**, 199 (1998) [arXiv:hep-th/9803015].

[26] M. Bershadsky, Z. Kakushadze and C. Vafa, "String expansion as large N expansion of gauge theories," Nucl. Phys. B **523**, 59 (1998) [arXiv:hep-th/9803076].

[27] M. Bershadsky and A. Johansen, "Large N limit of orbifold field theories," Nucl. Phys. B **536**, 141 (1998) [arXiv:hep-th/9803249].

[28] M. Schmaltz, "Duality of nonsupersymmetric large N gauge theories," Phys. Rev. **D59**, 105018 (1999) [arXiv:hep-th/9805218].

[29] J. Erlich and A. Naqvi, "Nonperturbative tests of the parent / orbifold correspondence in supersymmetric gauge theories," JHEP **0212**, 047 (2002) [arXiv:hep-th/9808026].

[30] M. J. Strassler, "On methods for extracting exact nonperturbative results in nonsupersymmetric gauge theories," [arXiv:hep-th/0104032].

[31] P. Kovtun, M. Ünsal and L. G. Yaffe, "Non-perturbative equivalences among large N(c) gauge theories with adjoint and bifundamental matter fields," JHEP **0312**, 034 (2003) [arXiv:hep-th/0311098].

[32] P. Kovtun, M. Ünsal and L. G. Yaffe, "Necessary and sufficient conditions for nonperturbative equivalences of large N(c) orbifold gauge theories," JHEP **0507**, 008 (2005) [arXiv:hep-th/0411177].

[33] P. Kovtun, M. Ünsal and L. G. Yaffe, "Can large N(c) equivalence between supersymmetric Yang-Mills theory and its orbifold projections be valid?," Phys. Rev. **D72**, 105006 (2005) [arXiv:hep-th/0505075].

[34] M. Ünsal and L. G. Yaffe, "(In)validity of large N orientifold equivalence," Phys. Rev. D **74**, 105019 (2006) [arXiv:hep-th/0608180].

[35] A. Cherman, M. Hanada and D. Robles-Llana, "Orbifold equivalence and the sign problem at finite baryon density," Phys. Rev. Lett. **106**, 091603 (2011) [arXiv:1009.1623 [hep-th]].

[36] A. Cherman, B. C. Tiburzi, "Orbifold equivalence for finite density QCD and effective field theory," [arXiv:1103.1639 [hep-th]].

[37] M. Hanada, C. Hoyos, A. Karch and L. G. Yaffe, "Holographic realization of large-Nc orbifold equivalence with non-zero chemical potential," [arXiv:1201.3718 [hep-th]].

[38] J. J. M. Verbaarschot and T. Wettig, "Random matrix theory and chiral symmetry in QCD," Ann. Rev. Nucl. Part. Sci. **50**, 343 (2000) [arXiv:hep-ph/0003017].

[39] G. Akemann, "Matrix models and QCD with chemical potential," Int. J. Mod. Phys. A **22**, 1077 (2007) [arXiv:hep-th/0701175].

[40] M. G. Alford, K. Rajagopal and F. Wilczek, "QCD at finite baryon density: Nucleon droplets and color superconductivity," Phys. Lett. B **422**, 247 (1998) [arXiv:hep-ph/9711395].

[41] R. Rapp, T. Schafer, E. V. Shuryak and M. Velkovsky, "Diquark Bose condensates in high density matter and instantons," Phys. Rev. Lett. **81**, 53 (1998) [arXiv:hep-ph/9711396].

[42] D. Weingarten, "Mass Inequalities For QCD," Phys. Rev. Lett. **51**, 1830 (1983).

[43] E. Witten, "Some Inequalities Among Hadron Masses," Phys. Rev. Lett. **51**, 2351 (1983).

[44] S. Nussinov, "Mass Inequalities In QCD," Phys. Rev. Lett. **52**, 966 (1984).

[45] D. Espriu, M. Gross and J. F. Wheater, "Rigorous Inequalities In Vector - Like Gauge Theories," Phys. Lett. B **146**, 67 (1984).

[46] T. Zhang, T. Brauner and D. H. Rischke, "QCD-like theories at nonzero temperature and density," JHEP **1006**, 064 (2010) [arXiv:1005.2928 [hep-ph]].

[47] S. Hands, I. Montvay, S. Morrison, M. Oevers, L. Scorzato and J. Skullerud, "Numerical study of dense adjoint matter in two color QCD," Eur. Phys. J. C **17**, 285 (2000) [arXiv:hep-lat/0006018].

[48] S. R. Coleman and E. Witten, "Chiral Symmetry Breakdown In Large N Chromodynamics," Phys. Rev. Lett. **45**, 100 (1980).

[49] M. E. Peskin, "The Alignment Of The Vacuum In Theories Of Technicolor," Nucl. Phys. B **175**, 197 (1980).

[50] A. Armoni, M. Shifman and G. Veneziano, "Exact results in non-supersymmetric large N orientifold field theories," Nucl. Phys. B **667**, 170 (2003) [arXiv:hep-th/0302163].

[51] I. Barbour, N. -E. Behilil, E. Dagotto, F. Karsch, A. Moreo, M. Stone and H. W. Wyld, "Problems with Finite Density Simulations of Lattice QCD," Nucl. Phys. B **275**, 296 (1986).

[52] D. Toublan, "A Large N(c) perspective on the QCD phase diagram," Phys. Lett. B **621**, 145 (2005) [arXiv:hep-th/0501069].

[53] D. T. Son, "Superconductivity by long-range color magnetic interaction in high-density quark matter," Phys. Rev. D **59**, 094019 (1999) [arXiv:hep-ph/9812287].

[54] T. Schäfer, "Patterns of symmetry breaking in QCD at high baryon density," Nucl. Phys. B **575**, 269 (2000) [arXiv:hep-ph/9909574].

[55] D. V. Deryagin, D. Y. Grigoriev and V. A. Rubakov, "Standing wave ground state in high density, zero temperature QCD at large N(c)," Int. J. Mod. Phys. A **7** (1992) 659.

[56] E. Shuster and D. T. Son, "On finite-density QCD at large N(c)," Nucl. Phys. B **573**, 434 (2000) [arXiv:hep-ph/9905448].

[57] E. V. Shuryak and J. J. M. Verbaarschot, "Random Matrix Theory And Spectral Sum Rules For The Dirac Operator In QCD," Nucl. Phys. A **560**, 306 (1993) [arXiv:hep-th/9212088].

[58] B. Klein, D. Toublan and J. J. M. Verbaarschot, "Diquark and pion condensation in random matrix models for two-color QCD," Phys. Rev. D **72**, 015007 (2005) [arXiv:hep-ph/0405180].

[59] M. A. Stephanov, "Random matrix model of QCD at finite density and the nature of the quenched limit," Phys. Rev. Lett. **76**, 4472 (1996) [arXiv:hep-lat/9604003].

[60] A. M. Halasz, A. D. Jackson, R. E. Shrock, M. A. Stephanov and J. J. M. Verbaarschot, "On the phase diagram of QCD," Phys. Rev. D **58**, 096007 (1998) [arXiv:hep-ph/9804290].

[61] A. M. Halasz, J. C. Osborn and J. J. M. Verbaarschot, "Random matrix triality at nonzero chemical potential," Phys. Rev. D **56**, 7059 (1997) [arXiv:hep-lat/9704007].

[62] J. C. Osborn, "Universal results from an alternate random matrix model for QCD with a baryon chemical potential," Phys. Rev. Lett. **93**, 222001 (2004) [arXiv:hep-th/0403131].

[63] G. Akemann, "The complex Laguerre symplectic ensemble of non-Hermitian matrices," Nucl. Phys. B **730**, 253 (2005) [arXiv:hep-th/0507156].

[64] B. Vanderheyden and A. D. Jackson, "Temperature dependence in random matrix models with pairing condensates," Phys. Rev. D **72**, 016003 (2005) [arXiv:hep-ph/0503156].

[65] H. Leutwyler and A. V. Smilga, "Spectrum of Dirac operator and role of winding number in QCD," Phys. Rev. D **46**, 5607 (1992).

[66] T. Kanazawa, T. Wettig and N. Yamamoto, "Chiral random matrix theory for two-color QCD at high density," Phys. Rev. D **81**, 081701 (2010) [arXiv:0912.4999 [hep-ph]].

[67] G. Akemann, M. J. Phillips and H. -J. Sommers, "Characteristic polynomials in real Ginibre ensembles," J. Phys. A, **42**, 012001 (2009) [arXiv:0810.1458 [math-ph]].

[68] G. Akemann, M. J. Phillips and H. -J. Sommers, "The Chiral Gaussian two-matrix ensemble of real asymmetric matrices," J. Phys. A **A43**, 085211 (2010) [arXiv:0911.1276 [hep-th]].

[69] T. Schäfer, "Instanton effects in QCD at high baryon density," Phys. Rev. D **65**, 094033 (2002) [arXiv:hep-ph/0201189].

[70] N. Yamamoto, "Instanton-induced crossover in dense QCD," JHEP **0812**, 060 (2008) [arXiv:0810.2293 [hep-ph]].

[71] N. Yamamoto and T. Kanazawa, "Dense QCD in a Finite Volume," Phys. Rev. Lett. **103**, 032001 (2009) [arXiv:0902.4533 [hep-ph]].

[72] T. Kanazawa, T. Wettig and N. Yamamoto, "Chiral Lagrangian and spectral sum rules for dense two-color QCD," JHEP **0908**, 003 (2009) [arXiv:0906.3579 [hep-ph]].

[73] J. Han and M. A. Stephanov, "A Random Matrix Study of the QCD Sign Problem," Phys. Rev. D **78**, 054507 (2008) [arXiv:0805.1939 [hep-lat]].

[74] P. de Forcrand, M. A. Stephanov and U. Wenger, "On the phase diagram of QCD at finite isospin density," PoS **LAT2007**, 237 (2007) [arXiv:0711.0023 [hep-lat]].

[75] J. B. Kogut and D. K. Sinclair, "Lattice QCD at finite temperature and density in the phase-quenched approximation," Phys. Rev. D **77**, 114503 (2008) [arXiv:0712.2625 [hep-lat]].

[76] P. de Forcrand and O. Philipsen, "The chiral critical line of $N_f = 2 + 1$ QCD at zero and non-zero baryon density," JHEP **0701**, 077 (2007) [arXiv:hep-lat/0607017].

[77] P. de Forcrand and O. Philipsen, "The chiral critical point of Nf=3 QCD at finite density to the order $(\mu/T)^4$," JHEP **0811**, 012 (2008) [arXiv:0808.1096 [hep-lat]].

[78] L. McLerran and R. D. Pisarski, "Phases of Cold, Dense Quarks at Large N_c," Nucl. Phys. A **796**, 83 (2007) [arXiv:0706.2191 [hep-ph]].

[79] T. Kojo, Y. Hidaka, L. McLerran and R. D. Pisarski, "Quarkyonic Chiral Spirals," Nucl. Phys. A **843**, 37 (2010) [arXiv:0912.3800 [hep-ph]].

[80] T. Sakai and S. Sugimoto, "Low energy hadron physics in holographic QCD," Prog. Theor. Phys. **113**, 843 (2005) [arXiv:hep-th/0412141].

[81] T. Imoto, T. Sakai and S. Sugimoto, "O(N) and USp(N) QCD from String Theory," Prog. Theor. Phys. **122**, 1433 (2010) [arXiv:0907.2968 [hep-th]].

[82] Y. Hidaka and N. Yamamoto, "A No-Go Theorem for Critical Phenomena in Large-Nc QCD," [arXiv:1110.3044 [hep-ph]].